Astronomy & Astrophysics

Star formation in Perseus⋆

V. Outflows detected by HARP

J. Hatchell[1] and M. M. Dunham[2]

[1] School of Physics, University of Exeter, Stocker Road, Exeter EX4 4QL, UK
e-mail: hatchell@astro.ex.ac.uk

[2] Department of Astronomy, The University of Texas at Austin, 1 University Station, C1400, Austin, Texas 78712-0259, USA

ABSTRACT

Aims. Molecular outflows provide an alternative method of identifying protostellar cores, complementary to recent mid-infrared studies. Continuing our studies of Perseus, we investigate whether all Spitzer-identified protostars, and particularly those with low luminosities, drive outflows and if any new protostellar cores (perhaps harbouring low-mass sources) can be identified via their outflows alone.

Methods. We have used the heterodyne array receiver HARP on JCMT to make deep ^{12}CO 3–2 maps of submm cores in Perseus, extending and deepening our earlier study with R×B and bringing the total number of SCUBA cores studied up to 83. Our survey includes 23/25 of the Spitzer low-luminosity objects believed to be embedded protostars, including three VeLLOs.

Results. All but one of the cores identified as harbouring embedded YSOs have outflows, confirming outflow detections as a good method for identifying protostars. We detect outflows from 20 Spitzer low-luminosity objects. We do not conclusively detect any outflows from IR-quiet cores, though confusion in clustered regions such as NGC1333 makes it impossible to identify all the individual driving sources. This similarity in detection rates despite the difference in search methods and detection limits suggests either that the sample of protostars in Perseus is now complete or that the existence of an outflow contributes to the Spitzer detectability, perhaps through the contribution of shocked H_2 emission in the IRAC bands. For five of the low-luminosity sources (including two previously believed to be embedded), there is no protostellar envelope detected at 350 μm and the Spitzer emission is entirely due to shocks. Additionally, we detect the outflow from IRAS 03282+3035 at 850 μm with SCUBA with 20–30% of the submm flux due to CO line contamination in the continuum passband.

Key words. star: formation – stars: evolution – submillimeter – ISM: jets and outflows

1. Introduction

An important aim of recent and upcoming submillimetre surveys of nearby star forming regions is to use the relative numbers of starless cores and protostars, compared to numbers and ages of the pre-main-sequence population, to determine the lifetimes of these early phases of star formation. These lifetimes measure the collapse timescale and therefore the strength of support against gravity. For accurate lifetimes, we need to differentiate between starless and protostellar cores in the submm population. There are two good methods of identifying protostellar cores: we can either look for an internal heating source, or evidence for an outflow.

In the era of the Spitzer space telescope, direct infrared detection of the hot dust heated by an embedded protostar has become by far and away the most popular detection method. Spitzer's ability to cover large areas of molecular clouds and identify protostellar sources within them is well documented, with many nearby molecular clouds now been covered in guaranteed time (Orion, Taurus), by the Cores to Disks programme (Evans et al. 2003) and its successor the Spitzer Gould's Belt Survey (Allen et al., in prep.). Although generally excellent, Spitzer identification is not infallible. Background galaxies are numerous and indistinguishable from protostars from their dust

emission alone. A protostellar spectrum does not directly prove that the source is embedded in the molecular cloud (a point discussed in detail in Dunham et al. 2008). Also, like many surveys, Spitzer is flux-limited, with a luminosity completeness limit of $0.004(d/140\,\mathrm{pc})^2\ L_\odot$ (Harvey et al. 2007; Dunham et al. 2008).

The Spitzer analysis has also raised some very interesting questions by detecting low luminosity objects (LLOs, with internal luminosities $L_{int} < 1\ L_\odot$) and very low luminosity objects (VeLLOs, $L_{int} < 0.1\ L_\odot$, Young et al. 2004; Dunham et al. 2008). These objects have typical spectra of Class 0 and I protostars, but luminosities which are far lower than one would expect from their mass. The nature of these sources is unclear. They may simply be forming very low mass stars, some may be very early Class 0 objects which have not yet reached their full luminosity, or they may currently be in a low accretion state (Dunham et al. 2008; Evans et al. 2009).

An alternative way of identifying embedded protostars is by detecting their outflows, either via high-excitation jet interactions (Herbig-Haro objects and shock-excited H_2; eg. Walawender et al. 2005a; Davis et al. 2008) or through low-excitation molecular lines such as ^{12}CO. Molecular outflows immediately identify a source as an embedded protostar, avoiding the contaminants of infrared colour selection, although confusion from neighbouring flows can be an issue, as we see below. Outflows are particularly interesting for VeLLO scenarios by identifying if the protostar has shown more active mass ejection

Table 1. Outflow status of SCUBA cores.

Source	RA(J2000)	Dec.(J2000)	$v_{\rm LSR}$	Receiver	Outflow?	Class	eYSO	Common name
(1)	(2)		(3)	(4)	(5)	(6)	(7)	(8)
HRF1	03:33:17.9	31:09:33.4	6.4	B	y	0 (000)	y	b1-c
HRF2	03:33:21.4	31:07:30.7	6.8	B	y	0 (000)	y	b1-bS
HRF4	03:33:16.3	31:06:54.3	6.7	B	y	0 (000)	y^b	b1-d
HRF5	03:33:01.9	31:04:23.2	6.6	HARP	n	S	n	
HRF7	03:33:16.5	31:07:51.3	6.6	B	y	I (III)	y	IRAS 03301+3057, B1 SMM6
HRF10	03:33:27.3	31:07:10.1	6.6	B	y	I (III)	y	B1 SMM11
HRF12	03:43:56.5	32:00:49.9	8.8	B,HARP	y,y	0 (000)	y^b	HH211
HRF13	03:43:56.9	32:03:04.8	8.6	B	y	0 (000)	y	IC348 MMS
HRF14	03:44:43.9	32:01:32.0	9.1	B	y	I (III)	y^b	
HRF15	03:43:50.8	32:03:24.2	8.8	B,HARP	y,y	0 (0I0)	y^b	IC348 SMM3
HRF16	03:44:01.0	32:01:54.8	8.8	B,HARP	n,n	S	n^b	
HRF17	03:43:57.9	32:04:01.5	8.4	B	$y?c13$	S	n	
HRF18	03:44:03.0	32:02:24.3	8.6	B,HARP	n,n	S	n	
HRF19	03:44:36.8	31:58:48.9	9.5	B,HARP	n,n	S	n	
HRF20	03:44:05.5	32:01:56.7	8.5	B,HARP	n,n	S	n	
HRF21	03:44:02.3	32:02:48.5	8.6	B,HARP	n,n	S	n	
HRF23	03:43:37.8	32:03:06.2	9.0	B,HARP	n	S	n	
HRF24	03:43:42.3	32:03:23.2	8.7	B,HARP	n,n	S	n	
HRF25	03:44:48.5	32:00:30.8	9.2	B,HARP	n,n	S	n	
HRF26	03:43:44.4	32:02:55.7	8.8	B	n	S	n	
HRF27	03:25:35.9	30:45:30.0	4.4	B	y	0 (000)	y	L1448 NW
HRF28	03:25:36.4	30:45:15.0	4.4	B	y	0 (0I0)	y^b	L1448 N A/B
HRF29	03:25:38.8	30:44:03.6	4.8	B	y	0 (000)	y^b	L1448C
HRF30	03:25:22.4	30:45:10.7	4.1	B	y	0 (000)	y	L1448 IRS2
HRF31	03:25:25.9	30:45:02.7	4.1	B	$y?c30$	0 (000)	n	
HRF32	03:25:49.0	30:42:24.6	4.4	HARP	$n?c27^a$	S	n	
HRF35	03:27:39.1	30:13:00.6	5.3	B	y	I (II0)	y	L1455 FIR4
HRF36	03:27:42.9	30:12:28.5	5.8	B	y	0 (0I0)	y	
HRF37	03:27:48.4	30:12:08.8	5.3	B	y	I (III)	y	L1455 PP9
HRF39	03:27:38.1	30:13:57.3	5.3	B	$y?c35$	I (I0I)	y^b	L1455 FIR1/2
HRF40	03:27:39.9	30:12:09.8	5.4	B	$y?c35,36$	S	n	
HRF41	03:29:10.4	31:13:30.0	7.6	B	y	0 (000)	y,0(6)	NGC1333 IRAS 4A
HRF42	03:29:12.0	31:13:10.0	7.5	B	y	0 (000)	$y,0(8)^b$	NGC1333 IRAS 4B
HRF43	03:29:03.2	31:15:59.0	7.9	B	y	I (III)	y,I(29)	NGC1333 SVS13
HRF44	03:28:55.3	31:14:36.4	7.7	B	y	0 (0I0)	$y,0(21)^f$	NGC1333 IRAS 2A
HRF45	03:29:01.4	31:20:28.6	7.6	B	y	I (III)	y,I(27)	NGC1333 ASR 114
HRF46	03:29:11.0	31:18:27.4	7.9	B	y	0 (000)	y,0(7)	NGC1333 ASR 32/33
HRF47	03:28:59.7	31:21:34.2	7.6	B	y	0 (000)	y,n	NGC1333 IRAS 4C
HRF48	03:29:13.6	31:13:55.0	7.6	B	$y?c41,42$	0 (000)	$y,0(9)^b$	NGC1333 SK31
HRF49	03:28:36.7	31:13:29.6	8.0	HARP	y	I (III)	y,I(15)	NGC1333 SK6
HRF50	03:29:06.5	31:15:38.6	7.9	B	$y?c43,51$	I (II0)	n,n	NGC1333 HH 7-11 MMS 4
HRF51	03:29:08.8	31:15:18.1	7.6	B	$y?c43,50$	S	n,n	NGC1333 SK16
HRF52	03:29:03.7	31:14:53.1	7.6	B	$y?c43,50$	0 (0I0)	y,0(5)	NGC1333 HH7–11 MMS 6
HRF53	03:29:04.5	31:20:59.1	7.6	B	$y?c45^d$	S	n,n	NGC1333 SK26
HRF54	03:29:10.7	31:21:45.3	7.6	HARP	$y? c56$	I (III)	n,n	NGC1333 SK28
HRF55	03:28:40.4	31:17:51.3	7.5	HARP	$y? c45,LL055$	0 (000)	$n,n^{b,g}$	
HRF56	03:29:07.7	31:21:56.8	7.6	HARP	y	I (III)	n,I(31)	NGC1333 SK29
HRF57	03:29:18.2	31:25:10.8	7.5	HARP	n	S	n,n	NGC1333 SK33
HRF58	03:29:24.0	31:33:20.8	7.5	HARP	$y?^a$	0 (I00)	$y,0(11)^b$	
HRF59	03:29:16.5	31:12:34.6	7.7	HARP	$y?c43^a$	S	n,n	
HRF60	03:28:39.4	31:18:27.1	8.4^c	HARP	$y?c45,LL066$	S	n,n	
HRF61	03:29:17.3	31:27:49.6	7.6	B,HARP	n,n	0 (000)	$y,0(10)^b$	
HRF62	03:29:07.1	31:17:23.7	7.9	B	$y?c46$	0 (0I0)	n,n	NGC1333 SK18
HRF63	03:29:18.8	31:23:16.9	7.2	HARP	$y?cBD +30° 549$	I (III)	y,n	NGC1333 SK32
HRF64	03:29:25.5	31:28:18.1	7.9	B,HARP	n,n	S	n,n	NGC1333 Per 4A3/4D
HRF65	03:29:00.4	31:12:01.5	7.9	HARP	y	0 (00I)	$y,0(4)^b$	NGC1333 IRAS 4B1
HRF66	03:29:05.3	31:22:11.3	7.6	HARP	$y?c56^a$	S	n,n	NGC1333 SK30
HRF67	03:29:19.7	31:23:56.0	7.5	HARP	y	I (III)	y,n	
HRF68	03:28:56.2	31:19:12.5	7.7	B	$y?c45$	0 (00I)	n,n^h	
HRF69	03:28:34.4	31:06:59.2	7.2^c	HARP	$y?c44$	I (I0I)	y,n	
HRF70	03:29:15.3	31:20:31.2	8.0^c	HARP	$y?c46$	0 (0I0)	n,n	NGC1333 SK22
HRF71	03:28:38.7	31:05:57.1	7.0^c	HARP	$y?cIRAS 03256+3055$	0 (000)	$y,0(1)^b$	NGC1333 HH 340B
HRF72	03:29:19.1	31:11:38.1	7.5	HARP	$y?c43^a$	S	n,n	

Table 1. continued.

Source	RA(J2000)	Dec.(J2000)	v_{LSR}	Receiver	Outflow?	Class	eYSO	Common name
(1)	(2)		(3)	(4)	(5)	(6)	(7)	(8)
HRF74	03:28:32.5	31:11:07.7	7.5^c	HARP	y	I (I0I)	y,I(12)^b	
HRF75	03:28:42.6	31:06:10.0	7.2^c	HARP	y	0 (000)	y,n^b	
HRF76	03:32:17.8	30:49:46.3	6.9	B	y	0 (I00)	y^b	IRAS 03292+3039
HRF77	03:31:21.0	30:45:27.8	7.2	B,HARP	y	0 (000)	y^b	IRAS 03282+3035
HRF78	03:47:41.6	32:51:44.0	10.0	B	y	I (III)	y	B5 IRS1
HRF79	03:47:39.1	32:52:17.9	10.0	B	n	S	n	
HRF80	03:26:37.6	30:15:24.2	5.0	HARP	$n,$y^a	I (III)	y^b	IRAS 03235+3004
HRF81	03:30:15.5	30:23:42.8	5.9	HARP	$n,$y?^{a}	I (III)	n	IRAS 03271+3013
HRF82	03:33:13.1	31:19:51.0	6.9	HARP	y^a	S	y	B1 SMM1
HRF83	03:32:48.9	31:09:40.1	6.0^c	HARP	n	S	n	
HRF84	03:32:21.9	31:04:55.6	6.0^c	HARP	n	0 (I00)	n	
HRF85	03:28:32.5	31:00:53.0	7.5	HARP	y?^{a}	S	n,I(13)	IRAS 03254+3050
HRF86	03:26:30.9	30:32:27.6	4.1	HARP	n	0 (000)	n	
HRF88	03:31:31.6	30:43:32.2	7.2^c	HARP	y?c77	0 (I00)	n	
HRF89	03:32:25.9	30:59:05.0	6.4	HARP	n	S	n	B1 SMM9
HRF90	03:45:16.5	32:04:47.1	10.0	HARP	n?^{a}	S	n	Per 7
HRF91	03:29:23.3	31:36:08.6	7.5^c	HARP	n	S	n	Per 4A
HRF101	03:44:12.8	32:01:33.9	8.6	HARP	y	I (III)	n	IRAS 03410+3152
Bolo11	03:25:46.5	30:44:17.8				S	n	
Bolo26	03:28:32.7	31:04:55.9	7.0	HARP	y?c65,NGC1333	S	n	
Bolo27	03:28:32.7	30:19:51.1				S	n	
Bolo44	03:29:04.9	31:18:41.2				S	n	
Bolo62	03:30:32.3	30:26:27.4	6.0^c	HARP	n	0 (I00)	n^b	
Bolo64	03:30:51.3	30:49:14.7	6.0^c	HARP	n	S	n	
Bolo70	03:32:44.3	31:00:09.7				S	n	
Bolo89	03:40:49.3	31:48:50.1				S	n	
Bolo90	03:41:09.3	31:44:38.1				I (III)	n	IRAS 03380+3135
Bolo92	03:41:40.7	31:57:59.8				S	n	
Bolo94	03:41:46.1	31:57:22.9				S	n	
Bolo111	03:44:14.4	31:57:57.6				S	n	
Bolo112	03:44:15.6	32:09:15.0				I (I0I)	n	
Bolo113	03:44:23.9	31:59:25.2				S	n^b	
Bolo114	03:44:23.2	32:10:10.1				S	n	
Bolo121	03:47:32.7	32:50:50.2				S	n	

[a] There are linewings which satisfy the low-level criterion – see Sect. 3.1.2. [b] Contains a Spitzer LLO (Dunham et al. 2008) – see Table 3. [c] Uncertain v_{LSR} due to broad and/or weak C^{18}O line, ^{13}CO detection only, or velocity taken from ^{12}CO itself. [d] At edge of mapped area. Possible S blue lobe. [e] Passed linewing criterion, but line profile suggests multiple velocity components rather than an outflow. [f] Gutermuth et al. (2008) Class 0 source 3 lies 30″ to the southeast of HRF44. [g] Gutermuth et al. (2008) Class I sources 16 and 18 lie 20″ to the south and 40″ to the southeast, respectively, of HRF55. [h] Gutermuth et al. (2008) Class I source 23 lies 15″ to the east of HRF68.

in the past, as momentum deposited at earlier times remains visible in the molecular outflow.

We have been studying star formation in the Perseus molecular cloud, the nearby star-forming region generating the young clusters IC348 and NGC1333 (Hatchell et al. 2005, 2007b,a; Hatchell & Fuller 2008, hereafter Papers I–IV). One of the aims has been to determine the pre/protostellar nature of the submm cores detected by SCUBA using outflows. This classification has been extensively studied using infrared data by Hatchell et al. (2007b) and the Spitzer teams (Jørgensen et al. 2007; Rebull et al. 2007; Gutermuth et al. 2008). In Paper III we published outflow maps of 54 submm cores out of a total of ∼100 in the cloud (drawing on the maps of Knee & Sandell 2000 for NGC1333). In this first outflow survey, out of 54 sources observed, 37 have broad linewings indicative of outflows and all but 4 of these are confirmed by Spitzer MIR detections. A simple lifetime analysis based on these data suggested that we were detecting about 50% as many starless cores as cores containing protostars in the SCUBA maps of this region, and therefore the prestellar lifetimes (above our submm detection limit) are shorter by a factor of 2 than the lifetimes of the protostars

(Paper III), in agreement with the recent Spitzer-based estimates Enoch et al. (2008); Evans et al. (2009).

However, in Paper IV we showed that the issue of pre/protostellar lifetimes is more complex. A plot of the fraction of protostellar cores as a function of core envelope mass (over a mass range from ∼10 $M_\odot$ to envelope mass below the substellar limit) shows that the fraction of protostellar cores is a strong function of core mass (Paper IV). The highest mass cores are all protostellar. One possible explanation is that massive cores evolve much more rapidly to form protostars than their low mass counterparts, and therefore we see few of them. At the other end of the distribution, the lower mass population is dominated by apparently starless cores, but the status of these cores is uncertain. As outflow mass scales with core mass, these cores fall below the completeness limit for our earlier outflows survey. It is also possible that they harbour low-luminosity sources below the completeness limit of Spitzer.

Motivated by the apparently large low-mass starless population and the intriguing VeLLOs, in this work we set out to determine the outflow status of the remaining SCUBA cores in our Perseus sample. This is only possible with a more sensitive

Table 2. Outflow detection statistics.

Type	Observed (HARP) (1)	Outflow (YSO?) (2)	Weak outflow (YSO?) (3)	Confused (YSO?) (4)	No outflow (YSO?) (5)
SCUBA cores					
Class 0	34 (14)	21 (2)[a]	1 (0)	8 (5)	4 (3)
Class I	20 (10)	13 (4)	2 (1)	5 (4)	0
Starless	29 (20)	0	2 (2)	8 (0)	19 (0)
Total	83 (42)	29 (9)	5 (3)	22 (9)	22 (3)
Low-luminosity objects					
LLOs	23 (12)	16 (0)[b]	2 (0)	2 (0)	3 (2)

[a] For SCUBA cores, the number in brackets indicate sources where there is disagreement on the protostellar status between Paper II, Jørgensen et al. (2007) and Gutermuth et al. (2008), as given in Table 1. [b] For LLOs the numbers in brackets indicate sources where there is no SHARC-II detection of a protostar.
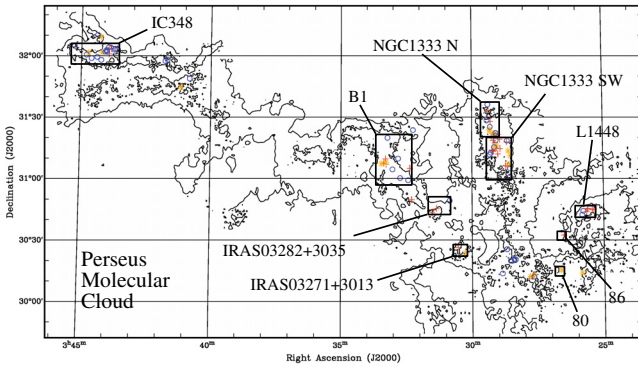
Fig. 1. Finding chart for the HARP outflow maps in Figs. 2–7. Contours show the molecular cloud in ^{13}CO integrated intensity (outer contour at 3 K km s^{-1}; map available from John Bally, at http://casa.colorado.edu/~bally/ftp/7mdata/Perseus_13co.fits) and C^{18}O for (inner contour 1 K km s^{-1}; Paper I). Class 0 and I protostars as identified by Paper II are shown as red/orange crosses/stars, and starless cores as blue circles.

survey than our earlier R×B work (0.3 K on 1 km s^{-1} channels), which pushes the completeness limit for outflows to lower mass. The new 16-receptor array receiver HARP-B on JCMT (Smith et al. 2008) has made this a real possibility, and in this work have applied it to make fully-sampled 2′ × 2′ maps, bringing the total number of cores covered to 83.

The structure of this paper is as follows. The HARP observations are described in Sect. 2 followed by the continuum observations with SHARC-II. Section 3 (Results) presents summary tables and discusses the outflow status for all the SCUBA cores in Perseus (Tables 1 and 2) and the low-luminosity Spitzer sources (Tables 2 and 3), along with the new HARP images (Figs. 2–7) and spectra (Figs. 8–9, available online only). Detailed discussion of individual sources, including the LLOs, is presented in the Appendix also included in the online version. In Sect. 3 we also present results on detection of lower-mass flows and the detection strategy for large-scale surveys such as JCMT Gould Belt Legacy Survey (GBS, Ward-Thompson et al. 2007), and CO contamination of the SCUBA 850 μm band in the IRAS 03282+3035 outflow. Finally, the implications for the detection of protostars via their outflows are discussed in Sect. 4.

Naming conventions. We identify SCUBA cores as HRF*nn* where *nn* is the number given in Paper I and Paper II; these can be found on SIMBAD as [HRF2005] *nn* or [HRF2007] *nn*. A few SCUBA cores which were originally found using Bolocam

are identified by their Enoch et al. (2006) numbers Bolo*nn* as in Paper II. Low-luminosity Spitzer objects are referred to as LL*nnn* following Dunham et al. (2008).

2. Observations

2.1. HARP

The observations were made with the 16-receptor Heterodyne Array Receiver Program *B*-band receiver (HARP-B, Smith et al. 2008) and ACSIS correlator (Dent et al. 2000; Lightfoot et al. 2000) on the James Clerk Maxwell telescope, Mauna Kea, Hawaii, between 22 September 2007 and 15 January 2008 (with the exception of HRF15 which was observed in Jan. 2007, and LL068,Bolo26 and LL090 which were observed in January 2009). We observed ^{12}CO $J = 3$–2 at 345 GHz with a dual subsystem backend with bandwidths (frequency resolutions) of 250 MHz (61 kHz) and 1 GHZ (0.977 MHz), giving a total velocity coverage of +/−400 km s^{-1} and velocity resolution in the inner ±100 km s^{-1} of 0.05 km s^{-1}. The array spacing is 30″ so to fully sample the 15″ JCMT beam we mapped using the "HARP-4" 16-position jiggle pattern with 7.5″ spacing. This resulted in 2′ × 2′ maps around each source position (sources marked HARP in Table 1). We also scan-mapped a larger, 8′ × 8′ area in the north of NGC1333 N, basket-weaving scans in RA and Dec offsetting by half the array size for each row. 14 of the 16 receptors were operational except for in 2009 where only 12 receptors were available. The mean of the array mean system temperatures was 377 K for the entire run, with mean standard deviations of 41 K across the array and 94 K over the run. Calibration was carried out using standard spectra on the proto-planetary nebula CRL618 and by observing a standard test position in Perseus B1 at the beginning of each observing session. Both the standard spectrum and the B1 test position were low in intensity on 10th October 2007 and intensities from this night have been increased by 20% to compensate. Data reduction was carried out using Starlink software[1].

A finding chart for the target regions is given in Fig. 1, and Figs. 2–7 show outflow maps based on the new HARP data.

2.2. SHARC-II

Submillimeter observations of select low luminosity objects (LLOs) at 350 μm were obtained with the Submillimeter High Angular Resolution Camera II (SHARC-II) at the Caltech Submillimeter Observatory (CSO) in November 2005, December 2006, October 2007, September 2008 and

---

[1] http://starlink.jach.hawaii.edu

Table 3. Outflow status of VeLLos and other low-luminosity embedded objects from Dunham et al. (2008).

LLO[1]	Spitzer ID[1]	Submm[2]	Instrument	Outflow?	SHARC-II[3]	Other names/location
(1)	(2)	(3)	(4)	(5)	(6)	(7)
VeLLos						
65	J032900.55+311200.7	HRF71	HARP	y?cLL068	y	southwest of NGC1333
73	J032912.07+311301.6	HRF42	B	y	–	NGC1333 IRAS4B
108	J034402.64+320159.5	HRF16	HARP	n	n	in IC348 horseshoe by 107
Low luminosity objects (Dunham et al. 2008 groups 1–4, probably embedded)						
55	J032536.22+304515.8	HRF28	B	y	–	L1448NW
56	J032539.12+304358.1	HRF29	B	y	–	L1448C
60	J032637.46+301528.1	HRF80	HARP	y	y	IRAS 03235+3004
63	J032738.26+301358.8	HRF39	B	y	–	L1455 FIR1/2
64	J032832.57+311105.3	HRF74	HARP	y	y	
68	J032845.29+310542.0	HRF75	HARP	y	y	30″ southeast of the submm peak
71	J032900.55+311200.7	HRF65	HARP	y	y	
74	J032913.54+311358.1	HRF48	B	y?[a] cHRF42	–	NGC1333 IRAS4C
75	J032917.16+312746.4	HRF61	HARP	n	y	N of NGC1333
78	J032923.47+313329.5	HRF58	HARP	y[b]	y	N of NGC1333
80	J032951.82+313906.1	–	–	–	–	Far north of NGC1333, outside SCUBA map.
81	J033032.69+302626.5	Bolo62	HARP	y?[b]cHRF81	y	NE of IRAS03271+3013 (HRF81)
84	J033120.98+304530.2	HRF77	B	y	–	IRAS03282+3035
88	J033217.95+304947.6	HRF76	B	y	–	IRAS03292+3039
90	J033229.18+310240.9	–	HARP	y	y	W of B1. Weak 850 μm emission peaks 10″ SSW.
92	J033314.38+310710.9	HRF4	B	y	–	NW of the submm peak
93	J033316.44+310652.6	HRF4	B	y	–	Coincident with submm peak
104	J034351.02+320307.9	HRF15	B/HARP	y	y	IC348-SMM3[c]
105	J034356.52+320052.9	HRF12	B	y	–	HH211
106	J034356.83+320304.7	HRF14	B	y	–	IC348 mms
107	J034402.40+320204.9	HRF16	HARP	n	n	in IC348 horseshoe by 108
109	J034421.36+315932.6	Bolo113	–	–		
Low Luminosity objects observed by HARP (groups 5–6, likely not embedded)						
66	J032843.58+311736.2	HRF55	HARP	y?c45	n	W of NGC1333
76	J032919.75+311256.9	–	HARP	y?c46,LL077	n	SW of NGC1333 IRAS4B
77	J032920.35+311250.4	–	HARP	y?c46,LL076	n	SW of NGC1333 IRAS4B

[a] The NGC1333 IRAS4C outflow status is uncertain from the R×B maps (Paper III). [b] Flows detected by the lower linewing criterion (Sect. 3.1.2).
[c] There is an additional Spitzer source to the north ("LL104N") which is not classified as a LLO but appears to be the outflow driving source.

October 2008. SHARC-II is a 12 × 32 element bolometer array giving a 2.59′ × 0.97′ field of view (Dowell et al. 2003). The beamsize at 350 μm is 8.5″. Approximate map fields of view ranged from ∼1′ to ∼10′, depending on the desired coverage for each source. During all observations the Dish Surface Optimization System (DSOS)[2] was used to correct the dish surface for gravitational deformations as the dish moves in elevation.

The raw scans were reduced with version 1.61 of the Comprehensive Reduction Utility for SHARC-II (CRUSH), a publicly available[3], Java-based software package. CRUSH iteratively solves a series of models that attempt to reproduce the observations, taking into account both instrumental and atmospheric effects (Kovács 2006; see also Kovács et al. 2006; Beelen et al. 2006). Pointing corrections to each scan were applied in reduction based on a model fit to all available pointing data (Dowell et al. 2009, private communication[4]). Pixels at the edges of the maps with a total integration time less than 25% of the maximum were removed to compensate for the increased noise in these pixels. We then used Starlink's *stats* package to assess the rms noise of each map, calculated using all pixels in the

off-source regions. A more complete description of the observation and data reduction strategy is given by Wu et al. (2007).

3. Results and discussion

We now have outflow observations of 83 submm cores in Perseus, as listed in Table 1. The JCMT Receiver B maps were published in Hatchell et al. (2007a) and the new HARP maps are shown in Figs. 2–7. In this section we first look at outflow identification, then the outflow detection statistics and how these compare with protostellar identifications from Spitzer. Secondly, we consider the outflows from Spitzer low-luminosity objects (Sect. 3.2). We then use these data to assess completeness to outflow detections in large ^{12}CO 3–2 surveys. Next, we discuss the evidence for CO line contamination of the SCUBA 850 μm band in the IRAS 03282 outflow. Finally, we consider the HARP maps region-by-region with notes on individual cores in Sect. A.

3.1. Outflows from SCUBA cores

Table 1 lists the outflow status for each of the 83 SCUBA cores now observed in ^{12}CO 3–2 (HARP and R×B). Left to right, the table columns are: (1) SCUBA source identifications from Paper I and Paper II; (2) 850 μm peak position from Paper II; (3) core velocity v_{LSR} mostly taken from C^{18}O 1–0 (details below);(4) JCMT receiver(s) (R×B and/or HARP) used for the outflow observations; (5) outflow detection status from R×B (italics) and HARP (roman font), where "y" indicates a detection
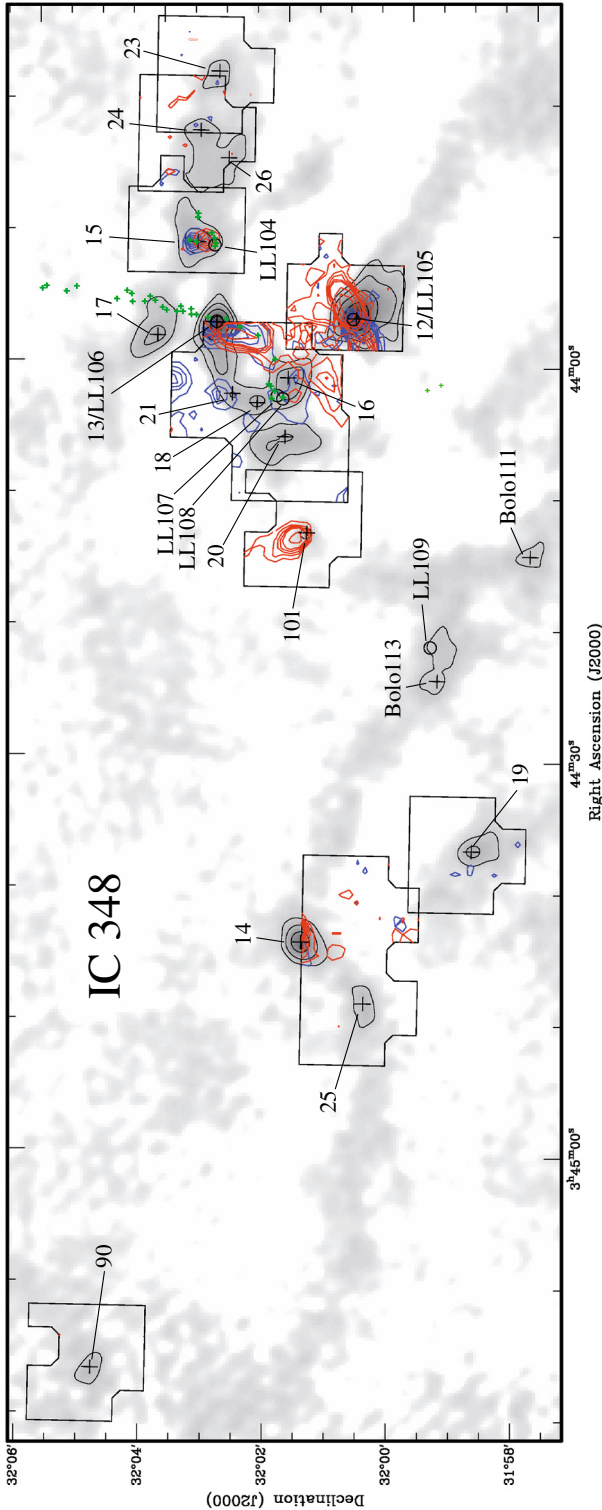
Fig. 2. Outflows in the IC348 filament, including continuum sources HRF12–20,23–26,90,101,Bolo111, and Bolo113 (labelled with black crosses +); and LL104–109 (black circles ○). The HARP fields are delineated in black. Greyscale: SCUBA 850 μm continuum with thin black contours at 100, 200, 400, 800, 1600, and 3200 mJy/beam. Red/blue contours: ^{12}CO 3–2 integrated intensity from $v-13$ km s^{-1} to $v-3$ km s^{-1} (blue) and $v+3$ km s^{-1} to $v+13$ km s^{-1} (red) where v is the line centre velocity as given in Table 1. Green crosses + mark the positions of H_2 shocks from Eislöffel et al. (2003). The data shown here are from HARP; additionally, R×B CO maps for sources 13 and 17 (with the rest of the HH211 horseshow) are found in Paper III. Contours are (1,2,3,4,5,10,20) K km s^{-1} except for HRF12/HH211, 16, 18, 20, and 21 where contours start at 2 K km s^{-1}).

by the standard or weak linewing criterion as described below, "n" no detection, and "y?" a confused flow with sources of confusion cnn as listed; (6) classification from Paper II, with sources classed as starless (S) if there is no infrared source or outflow, otherwise class 0 or I based on the evolutionary indicators $T_{\rm bol}$, $L_{\rm bol}/L_{\rm smm}$ and $F_{3.6}/F_{850}$; (7) embedded YSO classification from Jørgensen et al. (2007) and, for sources in NGC1333, YSO classification and identification from Gutermuth et al. (2008); and (8) common names.

3.1.1. Standard linewing criterion

The outflow detection status is based on our standard linewing criterion as used in Paper III. To classify a core, we first extract spectra at the submm peak position; these are shown in Fig. 8 (available in the online version). Then our standard criterion classifies sources with linewings above 1.5 K at 3 km s^{-1} from the core velocity $v_{\rm LSR}$ as outflow candidates. Core velocities are given in Table 1 and are taken from FCRAO C^{18}O spectra (Paper I) where possible, falling back on FCRAO ^{13}CO where the C^{18}O detection is too weak, and in a very few cases using the ^{12}CO line itself to estimate the velocity. Cores with outflow detections by the standard criterion are marked "y" in the outflow status column of Table 1.

We also consider whether the linewings could be due to confusion with flows from neighbouring sources. In crowded regions outflows cross other cores and lead to false positives, so we also use the outflow maps shown in Figs. 2–7 to identify possible sources of confusion. Cores where the linewings are possibly due to confusion are marked as questionable (y?) with the potential driving sources listed (cnn) in the outflow status column of Table 1.

3.1.2. Low-level linewing criterion

Our standard linewing criterion fails to detect any outflow from two Class 0 sources, HRF58 and HRF61, and two Class I sources, HRF80 (IRAS03235+3004) and HRF81 (IRAS 03271+3013). Many other Class I outflows lie at the detection limit. Looking at the spectra (Fig. 8, online) for these sources, there is clear evidence for linewings but they are below the 1.5 K level. In order to include these sources we try a lower level criterion of 0.3 K, ±4 km s^{-1}. All the Class I and HRF58 linewings are detected by this criterion, though not HRF61, though a higher signal-to-noise spectrum is needed to confirm this (currently, the rms is 0.38 K). With this more stringent criterion we also identify several more apparently starless sources as having linewings: HRF59, HRF66, HRF72, HRF82, and HRF85. These sources are marked as detections in Table 1 and identified as low-level detections in the footnotes. The detection for HRF90, which is an isolated source to the east of IC348, is almost certainly due to noise (σ = 0.27 K) and this is marked as a questionable non-detection in Table 1.

3.1.3. Outflow statistics

The outflow detection statistics for SCUBA cores and LLOs are summarised in Table 2. For each class of source (Class 0, I, starless, and/or LLO), the table lists the following : (1) total number of sources observed in ^{12}CO (in brackets, number observed by HARP); (2) number of sources with outflow linewing detections by the standard criterion and no confusion in the maps; (3) number of sources with outflow linewing detections by the low-level criterion and no confusion in the maps; (4) sources with outflow linewing detections by either criterion but maps
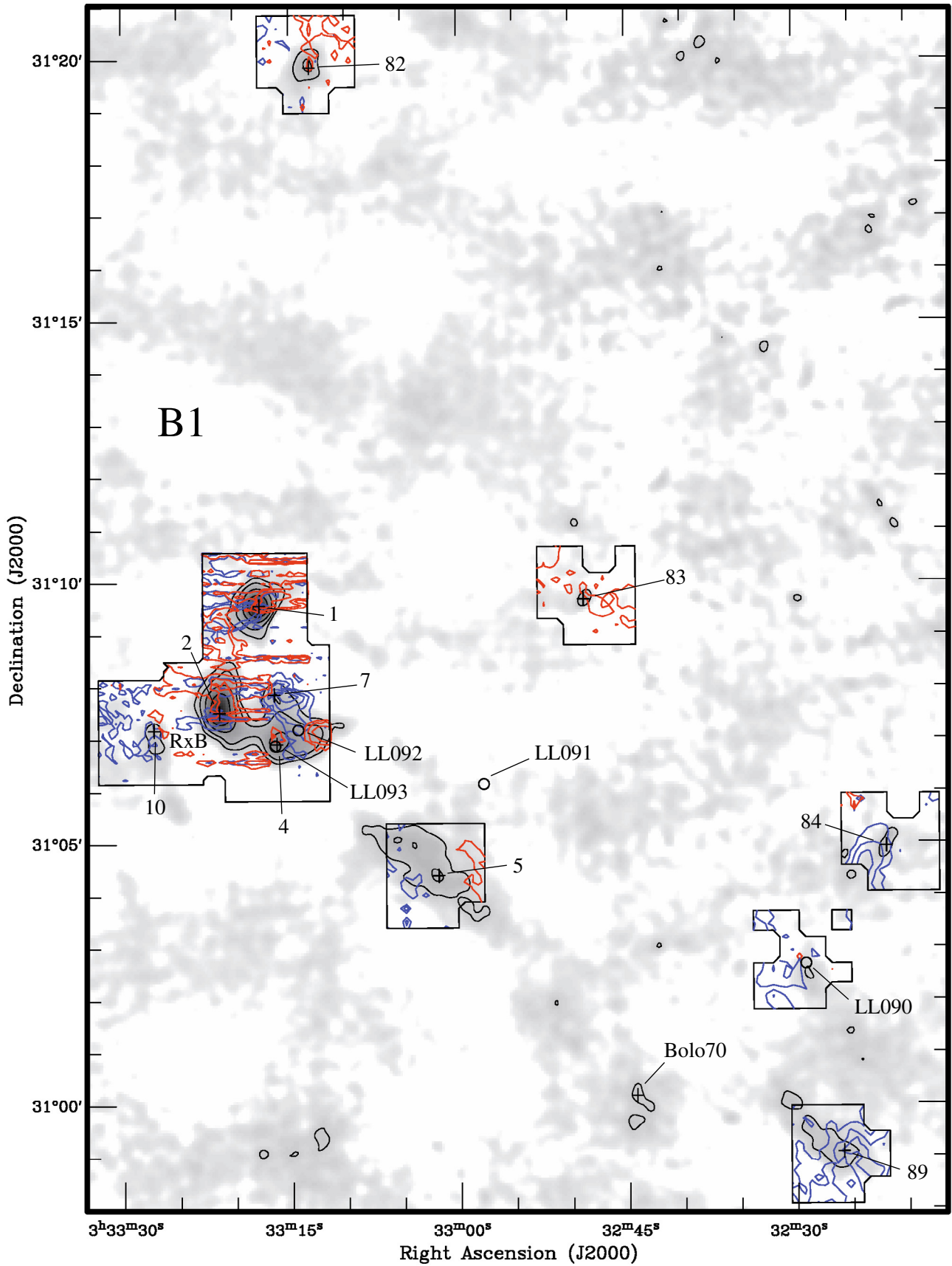
Fig. 3. Outflows in B1 and the filament to the southeast, including continuum sources HRF1, 2, 4, 5, 7, 10, 82, 83, 84, 89, Bolo70, and LL090-93. Greyscale and contours are as Fig. 2. All the detailed maps are from HARP; additionally for context, the overview shows the R×B map of the main B1 region from (Paper III), which also covered source HRF76 (IRAS 03292+3039). Contours are (1,2,3,4,5,10,20) K km s^{-1} except source 89 where contours start at 2 K km s^{-1}).
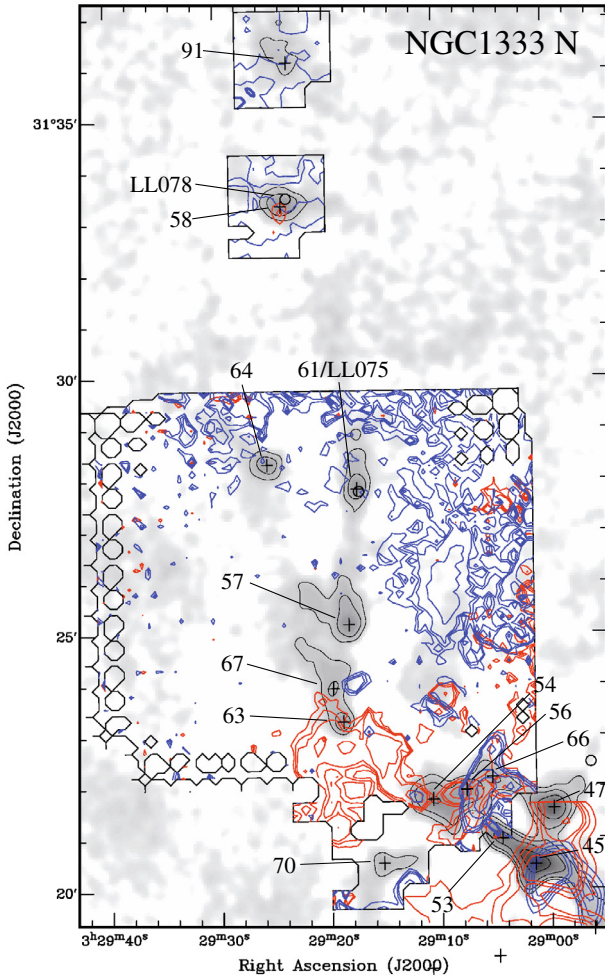
Fig. 4. Outflows in the region north of NGC1333, including sources HRF45,47,53,54,56,57,58,61,63,64,66,67,70, and 91; and LL075 and LL078. Greyscale and contours are as Fig. 2. All the detailed maps are from HARP; additionally for context, the overview shows the Knee & Sandell (2000) map of the main NGC1333 region (appearing in the bottom right corner). Contours in this region are (1,2,3,4,5,10,20) K km s^{-1} with contours in the main NGC1333 N region starting at 3 K km s^{-1}. See also the channel maps of this region in Fig. A.1.

show potential confusion with flows from another source; and (5) flows with no outflow. For SCUBA sources, the numbers in brackets on the last four columns indicate sources where there is disagreement on the protostellar status between Paper II, Jørgensen et al. (2007). For these sources, the outflow detection (or non-detection) provides additional evidence for the protostellar (or starless) status. For the LLOs, counts are only for sources which are probably embedded (Dunham et al. 2008 groups 1–4), and the numbers in brackets indicate sources with uncertain protostellar status because there is no SHARC-II detection of a protostar (see Sect. 3.2).

We detect outflows from all but four of the Hatchell et al. (2007b)-classified Class 0 sources. Three of these, HRF84,86 and Bolo62, have uncertain protostellar status and are probably starless. The remaining Class 0 source with no outflow detection is HRF61 in NGC1333 N, briefly mentioned above as the low-level non-detections in Sect. 3.1.2 and discussed in detail with the low-luminosity sources in 3.2, as it hosts LL075. One Class 0 source and two Class I sources have weak linewings detected at low level only: the Class 0 is HRF58, which hosts LL078 – see 3.1.2 and 3.2, and the Class I sources are

HRF81 (IRAS 03271+3013) and HRF80 (IRAS 03235+3004, LL060; Sect. 3.2). Including these, all the Class I sources have outflow identifications, and the Class 0 HRF61 is the only core unanimously agreed to be protostellar from Spitzer detections but with no outflow detection.

Even with the higher sensitivity of our HARP observations, there is no evidence that we detect any previously unknown protostars via their molecular outflows. The two starless sources with possible outflows are HRF85 and HRF82, both detected via low-level linewings, both of which were classified starless by Paper II but have since been suggested to host YSOs (Sect. 3.1.2, Sect. A.3 (HRF85) and Sect. A.5 (HRF82)).

The two cores hosting LLOs but without outflow detections are LLO75 (HRF61) in NGC1333 N, already discussed with the Class 0 sources above and in Sect. 3.1.2, and LL107/108 which we ascribe to H$_2$ shocks. The LLOs with weak outflow detections are the Class 0 source LL078 in HRF58 and the Class I source LL060 in HRF80. All of these sources are discussed further in Sect. 3.2.

In summary, our standard linewing condition identifies outflows for 87% of the Paper II Class 0 and Class I sources, rising to 93% if low-level linewing detections are included. If we only count sources which are unanimously agreed to be protostellar, from Spitzer and SCUBA observations, then the outflow detection rate is 97%, with only one non-detection (HRF61). There is a high level of confusion as to which outflow belongs to which source, and this is illustrated by the 34% "outflow detection" rate for cores classified starless on the Spitzer criteria. All of these apparent outflow detections are from starless sources in the NGC1333, IC348 and L1455 clusters and can be explained by confusion with other outflows from sources close by.

3.2. Low luminosity sources and VeLLOs

Our outflow survey includes many of the Spitzer-identified low luminosity objects (LLOs, which have internal luminosities $L_{int} < 1.0\ L_\odot$) and very low luminosity objects (VeLLOs, $L_{int} < 0.1\ L_\odot$) in the sample of Dunham et al. (2008). Of the 25 in Perseus which are known to be associated with high volume density, and therefore have a significant probability of being embedded sources (classified by Dunham et al. 2008 as Group 1–4 LLOs on this basis), 23 are covered by either our HARP or R×B surveys. In addition, our HARP maps also happen to cover three sources unlikely to be embedded sources (classified by Dunham et al. 2008 as Group 5–6 LLOs). The LLOs are mostly associated with SCUBA cores but are not identical with the SCUBA peak positions. Thus to apply the linewing criteria we have extracted spectra separately at the Spitzer positions (Fig. 9, online).

The outflow status for the LLOs are given in Table 3. Left to right, this table gives: (1) the LLO number from Dunham et al. (2008); (2) the Spitzer source identification; (3) the associated submillimetre source from Hatchell et al. (2005, 2007b) and Enoch et al. (2006); (4) the instrument (HARP or R×B) used for the ^{12}CO map; (5) outflow linewing detections as in Table 1, where "y" indicates a detection by the standard or weak linewing criterion, "n" no detection, and "y?" a confused flow with sources of confusion cnn as listed; (6) SHARC-II detections/non-detections at the LLO position, with a dash indicating no observation; and (7) other names and/or location of the source. A summary of the detection statistics for the LLOs believed to be embedded sources is given in Table 2.

Most of the low-luminosity objects observed by our earlier R×B study were well-known Class 0 sources with outflows. The
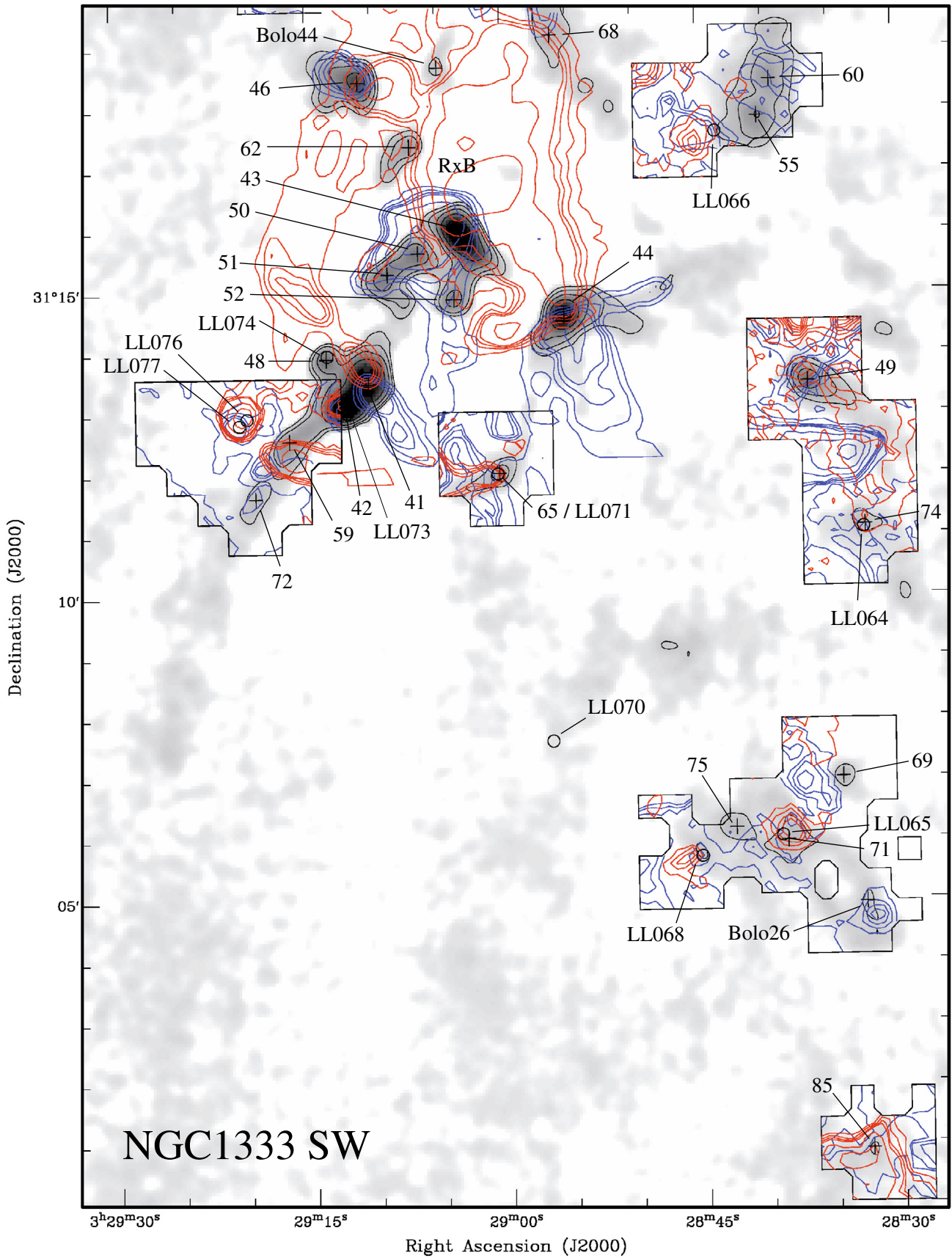
Fig. 5. Outflows in the south and west of NGC1333, including sources HRF41,42,44,46,48–52,54,55,59,60,62,65,68,69,71,72,74,75,85,Bolo26 and Bolo44; and LL064,LL065,LL066,LL068,LL070,LL071,LL074,LL076,and LL077. Greyscale and contours are as Fig. 2. All the detailed maps are from HARP; additionally for context, the overview shows the Knee & Sandell (2000) map of the main NGC1333 region. Contours in this region are (2,3,4,5,10,20) K km s^{-1} except field HRF65 where contours start at 1 K km s^{-1}.
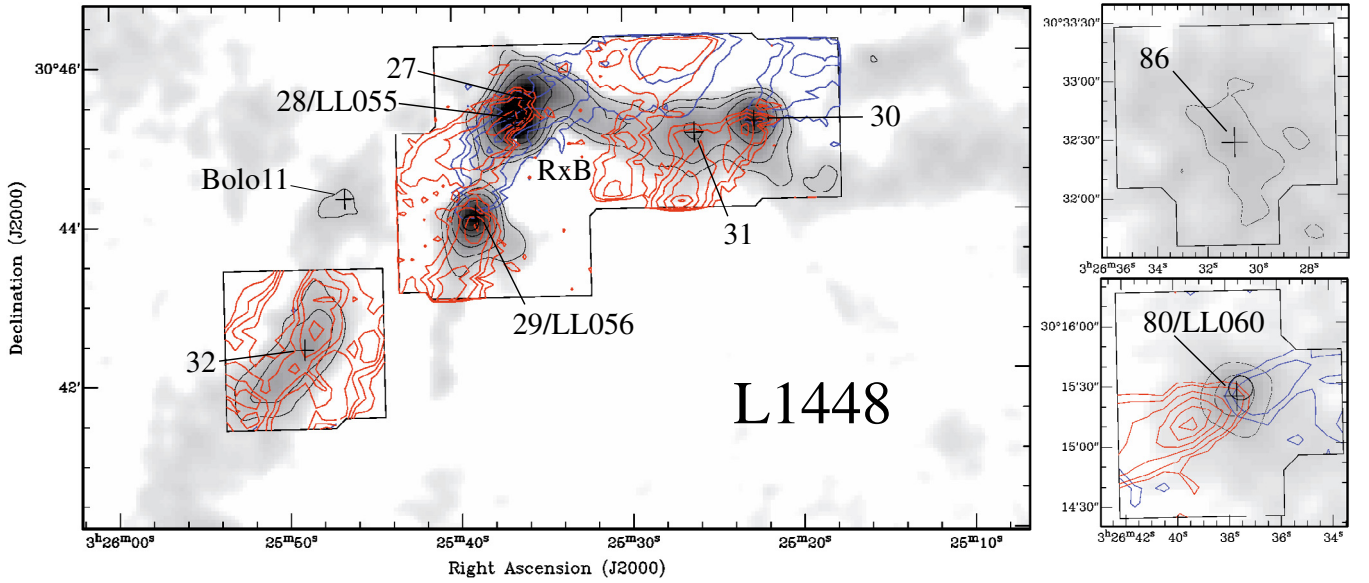
Fig. 6. Outflows in L1448, including sources HRF27–28, 30–32, 80 and 86, and Bolo11; and LL055, LL056 and LL060. Greyscale and contours are as Fig. 2. The detailed maps are from HARP; additionally for context, the overview shows the Paper III R×B map of the main L1448 region. Contours in this region are (0.5,1,2,3,4,5,10,20) K km s^{-1} starting at 0.5 K km s^{-1} for HRF80, 2 K km s^{-1} for HRF32, and 5 K km s^{-1} for the R×B map of L1448.
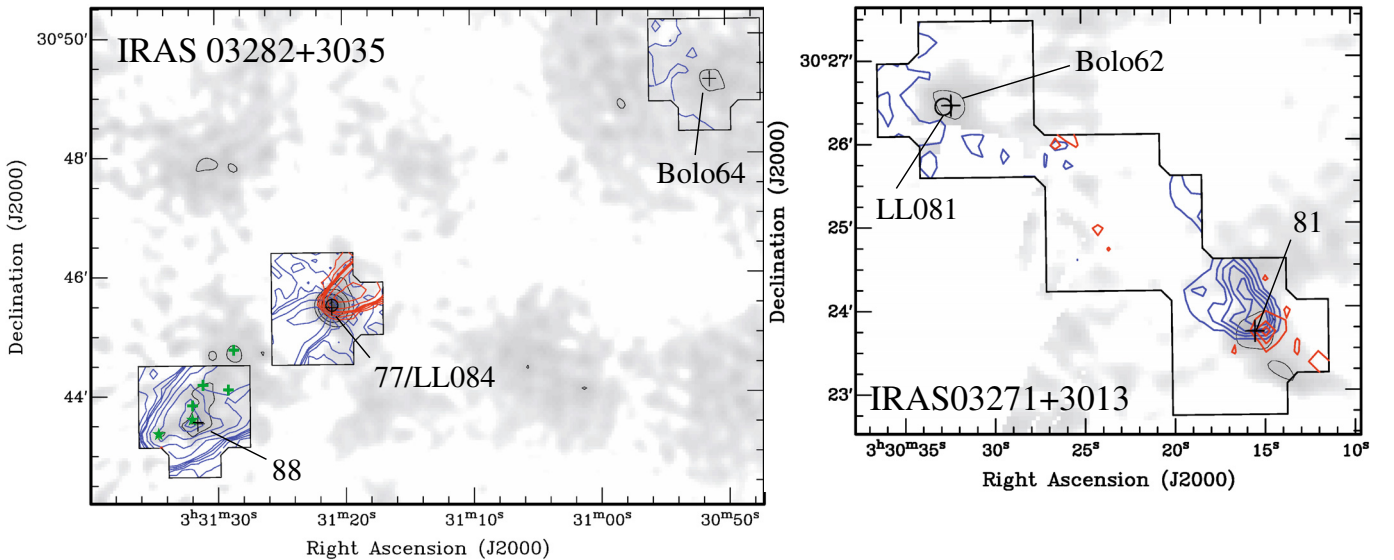
Fig. 7. Outflows from IRAS03282+3035, including sources HRF77,88, Bolo64 and LL084, and IRAS03272+3013, including sources HRF81, Bolo62 and LL081. Greyscale and contours are as Fig. 2. The H$_2$ and SiO peak positions from Bachiller et al. (1994) are marked by green crosses and stars, respectively. All the maps are from HARP. Contours are (1,2,3,4,5,10,20) K km s^{-1} except source 89 where contours start at 2 K km s^{-1}).

new, deep HARP observations are mainly of unstudied cores and include very low luminosity sources (VeLLOs, <0.1 $L_\odot$) 65 and 108. The new observations are examined source by source in Sect. A.1 of the Appendix and the reader should look there for detailed descriptions of individual objects. Here we look at the general properties of the LLOs in relation to outflows.

From our HARP and R×B observations, we find that most of the CO 3–2 spectra of the LLOs satisfy the standard linewing criterion (>1.5 K at 3 km s^{-1} from line centre, see Fig. 9 in the online version). Exceptions are LL075 (HRF61) in the far north of NGC1333 and LL107/LL108 in the IC348 horseshoe (see Sect. A.1). LL078 (HRF58) has a weak outflow which is detected with the low-level linewing criterion and visible in the maps (Fig. 4). This suggests that the majority of the LLOs are driving outflows, and that those outflows are not

particularly hard to detect. As already noted, many of the LLOs are massive Class 0 sources with well-known powerful flows: L1448 C (LL056), L1448 NW (LL055), L1455 FIR1/2 (LL063), NGC1333 IRAS4B (LL073), IRAS03282+3035 (LL084), IRAS03292+3039 (LL088), HH211 (LL105), and IC348 mms (LL106). We concentrate our efforts here on determining the status of the less well studied LLOs.

All four Spitzer IRAC bands, and particularly the 4.5 μm band, include emission lines of H$_2$ and other species which can be excited in shocks (Smith & Rosen 2005, 2007; Davis et al. 2008), as well as shock-excited continuum emission (Smith et al. 2006). Usually, H$_2$ shocks can be identified as such by their extended structure (the so-called "green fuzzies" or Extended Green Objects (EGOs); Cyganowski et al. 2008) but sometimes they can appear as compact sources. Therefore,
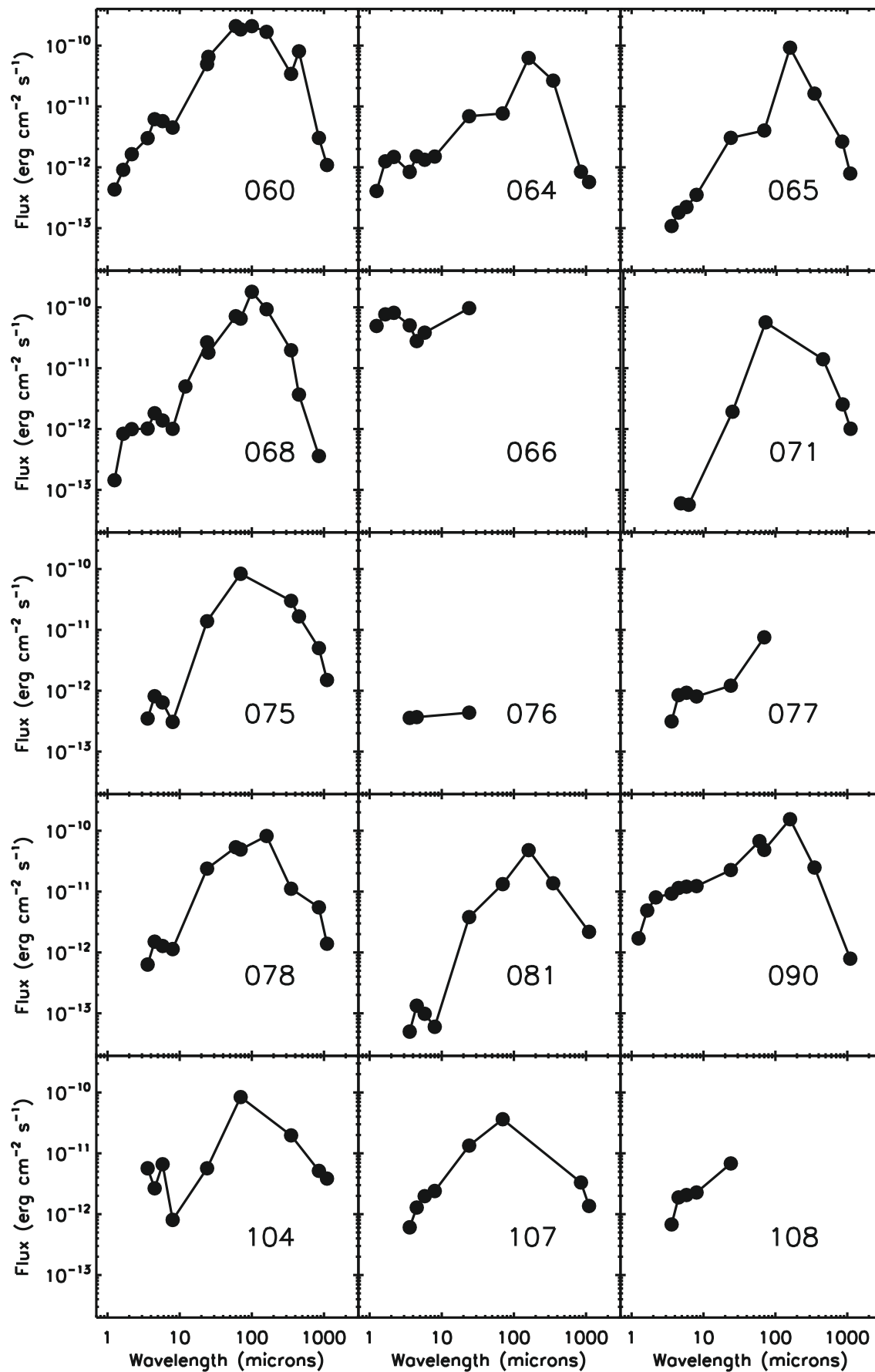
Fig. 10. Spectral energy distributions for the low-luminosity sources. Data are from 2MASS, Spitzer IRAC and MIPS, SHARC-II, SCUBA and Bolocam (Dunham et al. 2008).

some sources identified by Spitzer as YSOs may simply be H_2 knots with no local driving source (Davis et al. 2008). In outflows in local star-forming regions, the total luminosities in H_2 lines alone can reach 1 $L_\odot$ (Davis et al. 1997), comparable to the LLOs luminosities. This is a particular danger for the Perseus LLOs which lie in crowded regions where there are many outflows.

Unfortunately, IRAC colours alone are not sufficient to differentiate sources with and without driving sources. Fluxes rise steeply across the IRAC bands for an embedded protostar, and this is true for our LLOs, as shown in the SEDs in Fig. 10, though the fluxes have large uncertainties due to their faintness. Unfortunately, this is also predicted by H_2 shock/PDR excitation models (Smith et al. 2006), some of which produce colours which satisfy the Spitzer YSO candidate selection criteria (Harvey et al. 2007). Shocked H_2 is also common close to embedded protostars and the typical colours of embedded protostars reflect this (Davis et al. 2008). The weak IRAC fluxes are in any case uncertain and the 10 μm SiO absorption further complicates interpretation of the spectrum. Mid-IR spectra are needed to calculate the full contribution of lines to the continuum bands (Smith & Rosen 2005; Smith et al. 2006) but unfortunately these are not available for these sources. The predicted IRAC colours also vary greatly depending on the shock conditions (Smith & Rosen 2005; Smith et al. 2006). Some discrimination comes from the MIPS data as all of the LLOs require MIPS 24 μm and 70 μm detections, and there is no H_2 line in either of these bands. Faint 24 μm emission can be produced by [FeII] in shocks (Velusamy et al. 2007), and 70 μm emission by [OI] (Rebull et al. 2007). A strong detection in either of these bands is likely to indicate a central protostar, but these are lower-resolution bands and can suffer from confusion and saturation.

A true protostar will also produce a compact peak in the submm continuum emission, which can best be detected at shorter wavelengths (probing warmer dust) and higher resolution (for better discrimination from the background) than SCUBA 850 μm. We are fortunate enough to have 350 μm data from SHARC-II at the CSO, which has a 8.5″ beam at 350 μm, for most of the uncertain LLOs to use as a discriminant.

Figure 11 shows SHARC-II observations overlaid on the IRAC 4.5 μm emission. Most, but not all, of the low-luminosity sources do have compact 350 μm SHARC-II emission peaks coincident with the Spitzer sources, identifying these as protostars showing submm dust emission from compact envelopes as well as mid-IR emission indicating a central heating source.

The exceptional low-luminosity sources with no 350 μm detection are LL107/108, LL076/77, and LL066 (see Sect. A.1). The SHARC maps (Fig. 11) show that there is no 350 μm emission associated with LL076/77 to a level of 540 mJy/beam (3σ) or with LL066 to a level of 1.6 Jy/beam (3σ). Peak 350 μm fluxes, even for VeLLOs with $L < 0.1$ $L_\odot$ are typically more than 1 Jy and often much higher (Wu et al. 2007; Dunham et al. 2009). In both these cases, it is hard to see how this IRAC emission can be protostellar in origin, without a submm continuum detection of the surrounding envelope. However, they do coincide with H_2 shocks; both LL066 and LL076/77 are detected at 2.12 μm by Davis et al. (2008) and LL076/77 is associated with HH5 (Herbig 1974). In LL107/108, in the IC348 region to the north of HH211, the IRAC emission is definitely not coincident with the long-wavelength continuum peak (SHARC-II). The sources LL107/108 also coincide with known 2.12 micron H_2 emission (Eislöffel et al. 2003). For these five LLOs, the Spitzer emission is due to shocks and not to protostellar dust heating.

The Spitzer fluxes from LL107/108, LL076/77, and LL066 are examples of how emission from shocks can contribute significantly to the emission in the IRAC bands, and to a smaller extent in the 70 micron band, possibly simply due to dust heating. The fluxes in the IRAC bands are $\sim 10^{-12}$ erg cm^{-2} s^{-1}, similar to the fluxes from many other low-luminosity sources, and the SEDS (Fig. 10) show the characteristic YSO spectra rising through the IRAC and MIPS bands but are lacking submm emission (except for LL107/108, where it is misattributed; see Fig. 11). Even for the other low-luminosity sources which are genuinely protostellar, a significant fraction or even the majority of the IRAC band fluxes could be contributed by H_2 lines, enhancing their detectability.

Of the five LLOs which we now believe to be shocks, only LL107/108 were originally classified as likely to be embedded by Dunham et al. (2008), whereas three were not associated with dust emission. Thus we can have confidence that the contamination of the embedded LLO sample by shocks is small (2 out of 25 or 4%).

3.3. Outflow detection in large HARP surveys

Large area ^{12}CO surveys with HARP always have to strike a balance between mapping speed (and therefore area coverage) and sensitivity. The Sect. 3.1.2 low-level outflow detection criterion of 0.3 K at ± 4 km s^{-1} from line centre is, at 40 mn for a $2' \times 2'$ map, time-consuming to achieve in practice. It requires a sensitivity not always met even by our deep HARP observations. Large-area surveys work to lower sensitivities: for example, the JCMT Gould Belt Survey (GBS) is working to 0.3 K on 1 km s^{-1} for ^{12}CO 3–2 (Ward-Thompson et al. 2007), a factor of 4 shallower and similar to our old R×B data: is this sufficient to detect outflows?

In order to investigate how well outflows will be detected by the GBS and similar surveys, we added noise to the HARP outflow maps to match the GBS sensitivities of 0.3 K on 1 km s^{-1} and box smoothed them to 1 km s^{-1} resolution. Even with the added noise and degraded spectral resolution, we were still able to identify the same number of outflows using our standard linewidth criterion of 1.5 K at ± 3 km s^{-1}. This is not a complete surprise, given that these criteria were originally set for R×B spectra which had similar noise levels. However, of the weaker outflows discussed in Sect. 3.1.2 (HRF58, 80 and 81), only HRF58 could possibly have been detected in data with GBS noise levels. Applying the low-level linewidth criterion of 0.3 K at ± 4 km s^{-1} does not make sense for data with a noise level of 0.3 K rms.

Thus the GBS can therefore expect similar completeness statistics to those listed in Table 2, ie. a 87% detection rate for protostars and 35% false positives for starless cores. Strictly, these statistics are calculated for Perseus (250 pc from Černis & Straižys 2003 extinction studies), but we do not expect a strong distance dependence in the detectability of individual flows over the Gould Belt range (120–500 pc). This is because for extended sources like outflows the beam-averaged column density measured by CO spectra is roughly independent of distance. Only where outflows are significantly smaller (or narrower) than the beam does the detectability reduce with distance due to beam dilution. More of an issue at large distances is confusion where cores and outflows are less well resolved.

As Class I sources tend to have lower-mass CO outflows, there is a slight bias against detecting outflows from Class I sources. To be complete to outflows from the remaining protostars, a lower sensitivity of $1\sigma = 0.1$ K on 0.5 km s^{-1} channels
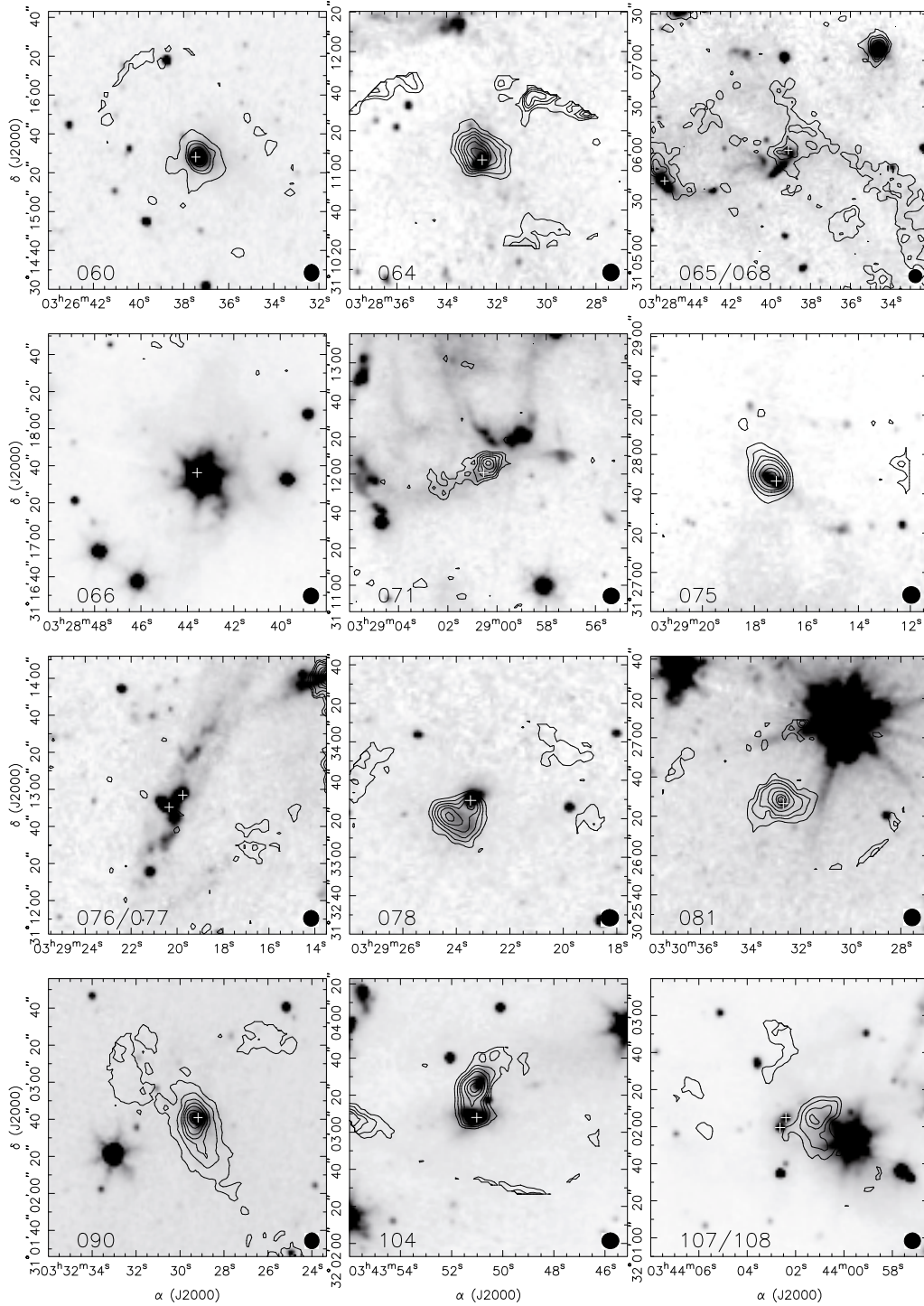
Fig. 11. Continuum emission associated with low-luminosity sources. Greyscale: IRAC 4.5 μm. Contours: 350 μm SHARC-II emission, with levels 2-σ plus 2σ for sources LL064(1σ 40 mJy/8.5″ beam), LL065/LL068 (90 mJy/beam), LL066 (535 mJy/beam), LL078 (55 mJy/beam), LL090 (55 mJy/beam) and LL107/108 (145 mJy/beam); 4σ plus 4σ for LL071 (180 mJy/beam) and LL076/077 (180 mJy/beam); 2,8,12,20,25,30,35σ for LL060 (65 mJy/beam); 2,4,6,8,12,16,20σ for LL075 and LL090 (1σ = 90 mJy/beam); and 2, 4, 6, 10, 14, 18, and 20σ for LL081 (35 mJy/beam).

is a good requirement. However, a deeper search is only worthwhile in relatively isolated cores, because in clustered regions such as NGC1333 and IC348, linewings from any low-mass outflows will be swamped by confusion with other more massive flows. As we do not detect any flows from sources without Spitzer detections, It is also most useful in regions where the YSOs have not already been identified, or as a confirmation of uncertain status.

3.4. Continuum detection of the IRAS 03282+3035 outflow: ^{12}CO 3–2 contamination in the 850 μm band

The southeast, blueshifted outflow lobe from IRAS 03282+3035 is detected by SCUBA at 850 μm(Fig. 7). SCUBA emission peaks at the main CO emission peak and at the jet head, with the 850 μm emission (greyscale / black contours in the figure) clearly showing a similar morphology to the CO. These positions also show strong SiO and H$_2$ emission (Bachiller et al. 1994).

There is further 850 μm emission associated with the Herbig-Haro object HH773 (Walawender et al. 2005b) and a linear H$_2$ shock further back towards the driving source.

Few examples of continuum emission in outflows have been studied before, with the notable exceptions of L1157 (Gueth et al. 2003) and V380 Ori-NE (Davis et al. 2000). There are two possible causes of 850 μm emission tracing an outflow: line contamination in the continuum bandpass, and/or dust heating by shocks.

From our HARP maps we can estimate the contribution of the CO line to the "continuum" flux by converting the line brightness temperature to intensity, averaging using the $\sim$60 GHz wide *SCUBA* filter passband, and multiplying by the beam area. The 850 μm flux per beam is then given by

$$\left(\frac{F_\nu}{\text{Jy beam}^{-1}}\right) = \frac{2k\nu^3}{c^3}\frac{g_\nu(\text{line})}{\int g_\nu d\nu}\Omega_B \int T_{\text{MB}}dv \tag{1}$$

where for SCUBA 850 μm $\nu(^{12}\text{CO 3-2}) = 345.7960$ GHz, g_ν is the filter transmission at frequency ν, $\int T_{\text{MB}}dv$ is the integrated main beam brightness temperature, and Ω_B is the JCMT beam at this frequency,

$$\Omega_B = \frac{\pi}{4\ln 2}\left(\frac{\theta_B}{''}\right)^2\left(\frac{\pi}{180\times 3600}\right)^2,$$

with θ_B the beam FWHM. A similar calculation is given by Seaquist et al. (2004) in calculating the CO 3–2 contribution to continuum for the SLUGS nearby galaxy sample. The *SCUBA* filters are available on the JCMT web pages[5]. Assuming a 15″ beam, an effective SCUBA 850 μm filter bandwidth of 59.4 GHz and 90% transmission at 345 GHz, we find a conversion factor of 0.383 mJy beam^{-1} (K km s^{-1})$^{-1}$ for ^{12}CO 3–2 in the 850 μm SCUBA passband.

The CO contamination from the ^{12}CO 3–2 integrated intensity of 142 K km s^{-1} is roughly 50 mJy/beam at the CO peak. At the jet head and HH773 peak we estimate a CO contribution of and 31 and 16 mJy beam^{-1} respectively. This compares to the measured SCUBA fluxes of 165, 155 and 103 $\pm$ 35 mJy beam^{-1} at the CO peak, jet head and HH773 peak respectively. Thus the CO emission contributes a significant fraction of the main peak 850 μm emission, of order 1/3, but less ($\sim$1/5) at the other positions. These are similar fractions to L1157, where Gueth et al. (2003) estimate 20% in the 850 μm passband, and V380 Ori-NE (Davis et al. 2000), where CO contamination is estimated to reach 50% in the outflow lobes.

Other lines in the band, for example SiO 8–7, will also contribute to the line contamination, though CO the only one for which we have a good measure of the integrated intensity. The total line contribution depends on the chemistry and excitation, but a factor of 2–3 times the CO line intensity is typical (Tothill et al. 2002 and references therein). Gueth et al. (2003) estimate that the total line contamination in the 1300 μm and 850 μm bands is a factor of 2 over that of CO. Therefore, it is possible that line emission accounts for all of the SCUBA 850 μm emission, especially given the large uncertainties in low-intensity SCUBA fluxes due to the unknown zero level and filtering to remove of large-scale fluctuations (Paper I)

On the other hand, the strongest 850 μm peaks are associated with shocked H$_2$ and SiO emission, rather than mirroring the CO contours. Enhancements at these specific positions are unlikely to be due to the random noise on the map, and suggests

that there is also heating of the dust by shocks. The estimated contribution from CO at these positions is low compared to the SCUBA detections (though note the 850 μm fluxes are quite uncertain). 850 μm emission is three times greater at 20 K compared to 10 K, increasing to a factor of 11 at 50 K, so moderate heating could easily lead to a SCUBA detection.

Thus we conclude that a combination of ^{12}CO 3–2 contamination of up to 30%, plus other lines in the band, plus dust heating by shocks, explains the SCUBA 850 μm emission from this outflow. Gueth et al. (2003) drew similar conclusions for L1127.

There is no detection of the outflow at 350 μm from SHARC-II, although the IRAS03282+3035 driving source is clearly detected. It is possible in principle that the CO J = 7–6 line (806 GHz) could contaminate the SHARC-II continuum (780–910 GHz, Dowell et al. 2002), in the same way that CO 3–2 contaminates SCUBA 850 μm. Measurements of CO 7–6 at these positions do not exist, but for a typical 100 K km s^{-1} CO 7–6 integrated intensity we calculate a contribution of less than 100 mJy/beam in the *SHARC-II* band. Our SHARC-II maps of the IRAS03282+3035 region, taken in poor weather, are not sensitive enough to detect this level of emission. 100 mJy/beam is also much less than the observed 350 μm peak fluxes for LLOs of typically 1 Jy/beam (Fig. 11). Thus CO 7–6 may contribute $\sim$20% of the continuum emission in the 350 μm band, though we have no direct evidence for this.

The redshifted counterpart flow to the northwest of IRAS 03282 is obvious in Spitzer IRAC maps (Jørgensen et al. 2007) in addition to the original CO detections (Bachiller et al. 1991) but there is no dust continuum detected by SCUBA. Continuum source Bolo84 lies directly on its path but is weak in ^{12}CO with no significant linewings which would indicate interaction with the flow (see Figs. 8, in the online version, and 7). The bandpass of Bolocam (250–300 GHz, Glenn et al. 2003) does not include any ^{12}CO lines, so any outflow contribution to Bolocam emission would have to be from hot dust.

The 850 μm detection of the outflow from IRAS03282+3035 raises the question of whether other flows in Perseus also show emission in this band. Generally, from Eq. (1), any outflow with typical ^{12}CO 3–2 line strengths $\geq$10 K and line widths $\geq$10 km s^{-1} will contribute at few tens of mJy to the 850 μm continuum. With contributions from CO measured in tens of mJy, even for strong outflows, and a rms on the Perseus SCUBA map 35 mJy/beam, we are near the detection limit for CO in the 850 μm maps and it is hard to be conclusive about matches in morphology. Additionally, the HARP maps presented here only cover small areas and near the driving sources one expects to see dust genuinely tracing the outflow cavity; it is further out from the cores that the CO contribution can become dominant. Nonetheless, there are some good candidates in L1448: the filament to the south of L1448 C (HRF29) tracks the outflow from this source; there is a 850 μm extension to the south tracking the outflow from L1448 IRS1 (HRF36); and HRF32 (mapped here) lies on the L1448 N/NW (HRF27/28) flow. Close to IRAS 03271+3013 (HRF81) the CO flow is traced by 850 μm emission. In all these cases, the 850 μm emission may include a contribution from the CO 3–2 line. The other powerful flows in Perseus mostly lie in NGC1333, which is so confused that it is hard to draw any conclusions. Overall, the maps are consistent with dust continuum emission appearing where there is strong ^{12}CO 3–2 emission (>20 K km s^{-1} in the linewings). This is not very significant in our SCUBA maps of Perseus, with a 3σ detection level of 105 mJy beam^{-1}, but in the deeper continuum maps planned with SCUBA-2 (which has similar filters) outflow detections should become common.

---

[5] http://www.jach.hawaii.edu

4. Conclusions

This paper completes our study of outflows from SCUBA cores in Perseus (Paper III), taking the total number of cores mapped in ^{12}CO 3–2 up to 83. We draw the following conclusions:

- CO 3–2 outflow maps are confirmed as a good tool for identifying protostars. All but one of the 35 submm cores unanimously classified as protostellar by Spitzer has an outflow linewing detection. The single exception is source HRF61 to the north of NGC1333 where the molecular gas may be destroyed and dissipated by the B stars in the main cluster.

- Confusion is a major difficulty for classifying cores in clustered regions where cores and flows often overlap in projection. Confusion leads to a large fraction of false positives; in Perseus, which includes the large NGC1333 and IC348 clusters, 35% of cores which are classified starless from submm/Spitzer comparisons exhibit broad linewings.

- Broad linewings characteristic of outflows are detected for all but three of the Spitzer low luminosity objects believed to be embedded sources (Dunham et al. 2008). Two of these are misidentifications due to H_2 in the Spitzer bands and one is the NGC1333 N source HRF61 mentioned above.

- It is remarkable that Spitzer and ^{12}CO 3–2 maps identify the same cores as protostars despite the difference in technique and differing detection limits. We would like to believe that this indicates that the list of Spitzer-detected protostars in Perseus is complete. However, there remains the possibility that IRAC detectability is linked to the presence of an outflow due to the luminosity of shocked H_2 emission in the IRAC bands.

- H_2 emission in the Spitzer IRAC bands potentially leads to outflow shocks being classified as low-luminosity protostars. This is mitigated by the Spitzer YSO requirement for MIPS 24 and 70 μm emission and compact, rather than extended, sources, and can be checked by looking for a 350 μm counterpart. We identify five Spitzer LLOs which lack 350 μm emission and are probably H_2 shocks rather than protostars. Two of these, including one VeLLO, were believed to be embedded YSOs.

- ^{12}CO 3–2 emission can lead to detection of outflows in the SCUBA 850 μm band and potential identification as spurious submm cores. We predict that detection of outflows with fluxes of a few tens of mJy will be common with SCUBA-2 surveys working to less than 10 mJy/beam at 850 μm. Maps of ^{12}CO 3–2 are a useful tool in assessing the magnitude of line contamination.

- Large ^{12}CO 3–2 surveys of local star-forming regions should detect the majority of outflows if they work to a sensitivity of 0.3 K on 1 km s^{-1} (eg. the JCMT GBS, Ward-Thompson et al. 2007). In Perseus (320 pc) we are 87% complete to protostars at this sensitivity.

- This study has not conclusively identified outflows from any cores previously believed to be starless. Thus, the starless/protostellar populations for Perseus remain unchanged, and the difference between the mass distributions for starless and protostellar cores – that the most massive cores are protostellar and there is an excess of low-mass starless cores – still holds (see Paper IV and Enoch et al. 2007). This rules out a simple one-to-one mapping between the prestellar core mass function and the stellar IMF.

References

Aspin, C. 2003, AJ, 125, 1480
Bachiller, R., Martin-Pintado, J., Tafalla, M., Cernicharo, J., & Lazareff, B. 1990, A&A, 231, 174
Bachiller, R., Andre, P., & Cabrit, S. 1991, A&A, 241, L43
Bachiller, R., Terebey, S., Jarrett, T., et al. 1994, ApJ, 437, 296
Beelen, A., Cox, P., Benford, D. J., et al. 2006, ApJ, 642, 694
Cohen, M., Jones, B. F., & Hereld, M. 1991, ApJ, 371, 237
Cyganowski, C. J., Whitney, B. A., Holden, E., et al. 2008, AJ, 136, 2391
Davis, C. J., Ray, T. P., Eisloeffel, J., & Corcoran, D. 1997, A&A, 324, 263
Davis, C. J., Dent, W. R. F., Matthews, H. E., Coulson, I. M., & McCaughrean, M. J. 2000, MNRAS, 318, 952
Davis, C. J., Scholz, P., Lucas, P., Smith, M. D., & Adamson, A. 2008, MNRAS, 387, 954
Dent, W., Duncan, W., Ellis, M., et al. 2000, in Imaging at Radio through Submillimeter Wavelengths, ed. J. G. Mangum, & S. J. E. Radford, ASP Conf. Ser., 217, 33
Dowell, C. D., Allen, C. A., Babu, R. S., et al. 2003, in SPIE Conf. Ser. 4855, ed. T. G. Phillips, & J. Zmuidzinas, 73
Dunham, M., Evans, N. I., & coauthors. 2009, in prep.
Dunham, M. M., Crapsi, A., Evans, II, N. J., et al. 2008, ApJS, 179, 249
Eislöffel, J., Froebrich, D., Stanke, T., & McCaughrean, M. J. 2003, ApJ, 595, 259
Enoch, M. L., Young, K. E., Glenn, J., et al. 2006, ApJ, 638, 293
Enoch, M. L., Glenn, J., Evans, II, N. J., et al. 2007, ApJ, 666, 982
Enoch, M. L., Evans, II, N. J., Sargent, A. I., & Glenn, J. 2008, ArXiv e-prints
Evans, N. J., Allen, L. E., Blake, G. A., et al. 2003, PASP, 115, 965
Evans, N. J., Dunham, M. M., Jørgensen, J. K., et al. 2009, ApJS, 181, 321
Glenn, J., Ade, P. A. R., Amarie, M., et al. 2003, in SPIE Conf. Ser. 4855, ed. T. G. Phillips, & J. Zmuidzinas, 30
Gueth, F., Bachiller, R., & Tafalla, M. 2003, A&A, 401, L5
Gutermuth, R. A., Myers, P. C., Megeath, S. T., et al. 2008, ApJ, 674, 336
Harvey, P., Merín, B., Huard, T. L., et al. 2007, ApJ, 663, 1149
Hatchell, J., & Fuller, G. A. 2008, A&A, 482, 855 (Paper IV)
Hatchell, J., Richer, J. S., Fuller, G. A., et al. 2005, A&A, 440, 151 (Paper I)
Hatchell, J., Fuller, G. A., & Richer, J. S. 2007a, A&A, 472, 187 (Paper III)
Hatchell, J., Fuller, G. A., Richer, J. S., Harries, T. J., & Ladd, E. F. 2007b, A&A, 468, 1009 (Paper II)
Herbig, G. H. 1974, Lick Observatory Bulletin, 658, 1
Hodapp, K. W., Bally, J., Eislöffel, J., & Davis, C. J. 2005, AJ, 129, 1580
Jørgensen, J. K., Johnstone, D., Kirk, H., & Myers, P. C. 2007, ApJ, 656, 293
Knee, L. B. G., & Sandell, G. 2000, A&A, 361, 671
Kovács, A. 2006, Ph.D. Thesis, Caltech, email:attila@submm.caltech.edu
Kovács, A., Chapman, S. C., Dowell, C. D., et al. 2006, ApJ, 650, 592
Lada, C. J., Alves, J., & Lada, E. A. 1996, AJ, 111, 1964
Lightfoot, J. F., Dent, W. R. F., Willis, A. G., & Hovey, G. J. 2000, in Astronomical Data Analysis Software and Systems IX, ed. N. Manset, C. Veillet, & D. Crabtree, ASP Conf. Ser., 216, 502
Loren, R. B. 1976, ApJ, 209, 466
Rebull, L. M., Stapelfeldt, K. R., Evans, II, N. J., et al. 2007, ApJS, 171, 447
Sandell, G., & Knee, L. B. G. 2001, ApJ, 546, L49
Seaquist, E., Yao, L., Dunne, L., & Cameron, H. 2004, MNRAS, 349, 1428
Smith, H., Buckle, J., Hills, R., et al. 2008, in SPIE Conf. Ser. 7020
Smith, H. A., Hora, J. L., Marengo, M., & Pipher, J. L. 2006, ApJ, 645, 1264
Smith, M. D., & Rosen, A. 2005, MNRAS, 357, 1370
Smith, M. D., & Rosen, A. 2007, MNRAS, 378, 691
Strom, S. E., Vrba, F. J., & Strom, K. M. 1976, AJ, 81, 314
Tafalla, M., Kumar, M. S. N., & Bachiller, R. 2006, A&A, 456, 179
Tothill, N. F. H., White, G. J., Matthews, H. E., et al. 2002, ApJ, 580, 285
Černis, K., & Straižys, V. 2003, Baltic Astronomy, 12, 301
Velusamy, T., Langer, W. D., & Marsh, K. A. 2007, ApJ, 668, L159
Walawender, J., Bally, J., Kirk, H., & Johnstone, D. 2005a, AJ, 130, 1795
Walawender, J., Bally, J., & Reipurth, B. 2005b, AJ, 129, 2308
Walawender, J., Bally, J., Kirk, H., et al. 2006, AJ, 132, 467
Walsh, A. J., Myers, P. C., Di Francesco, J., et al. 2007, ApJ, 655, 958
Ward-Thompson, D., Di Francesco, J., Hatchell, J., et al. 2007, PASP, 119, 855
Wilking, B. A., Meyer, M. R., Greene, T. P., Mikhail, A., & Carlson, G. 2004, AJ, 127, 1131
Wolf-Chase, G. A., Barsony, M., & O'Linger, J. 2000, AJ, 120, 1467
Wu, J., Dunham, M. M., Evans, II, N. J., Bourke, T. L., & Young, C. H. 2007, AJ, 133, 1560
Young, C. H., Jørgensen, J. K., Shirley, Y. L., et al. 2004, ApJS, 154, 396
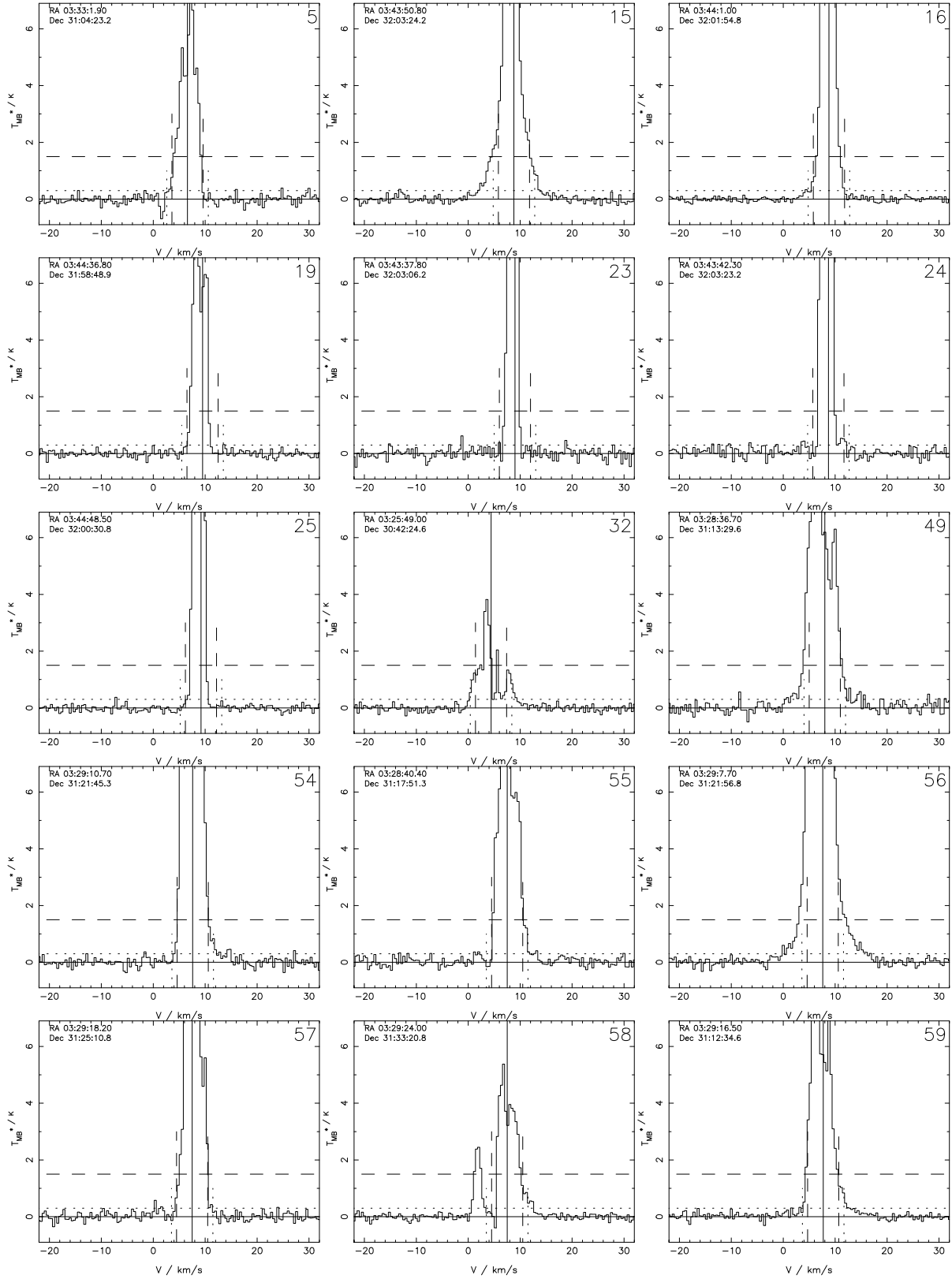
Fig. 8. ^{12}CO spectra at the positions of the SCUBA peaks. The line centre velocity is marked with a solid vertical line. The standard linewing criteria of 15 K at 3 km s^{-1} is marked with long dashes, and the low-level linewing criteria with short dashes. The positions at which the spectra were extracted are given in the top left. Available in the online version only.
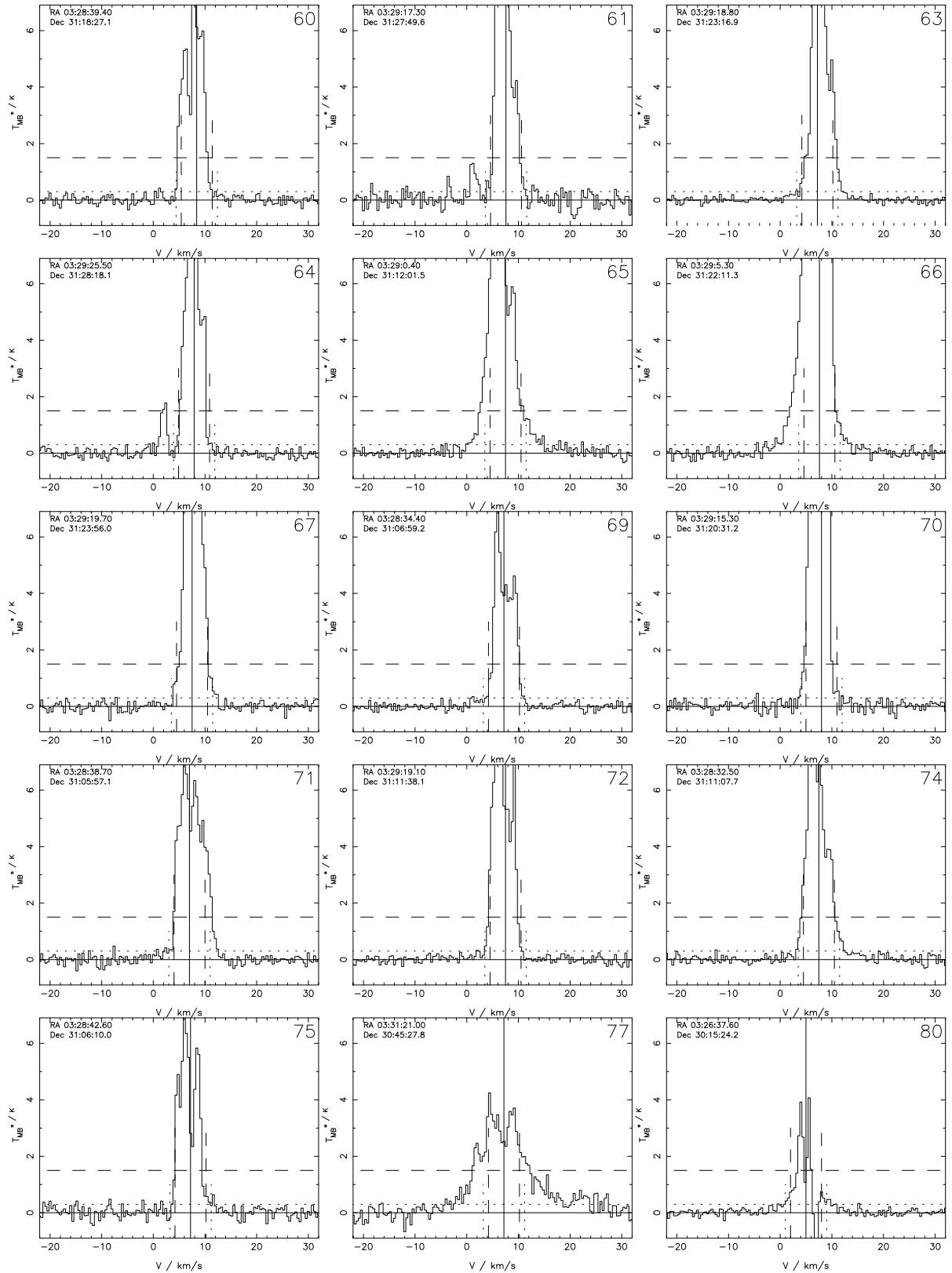
Fig. 8. continued.
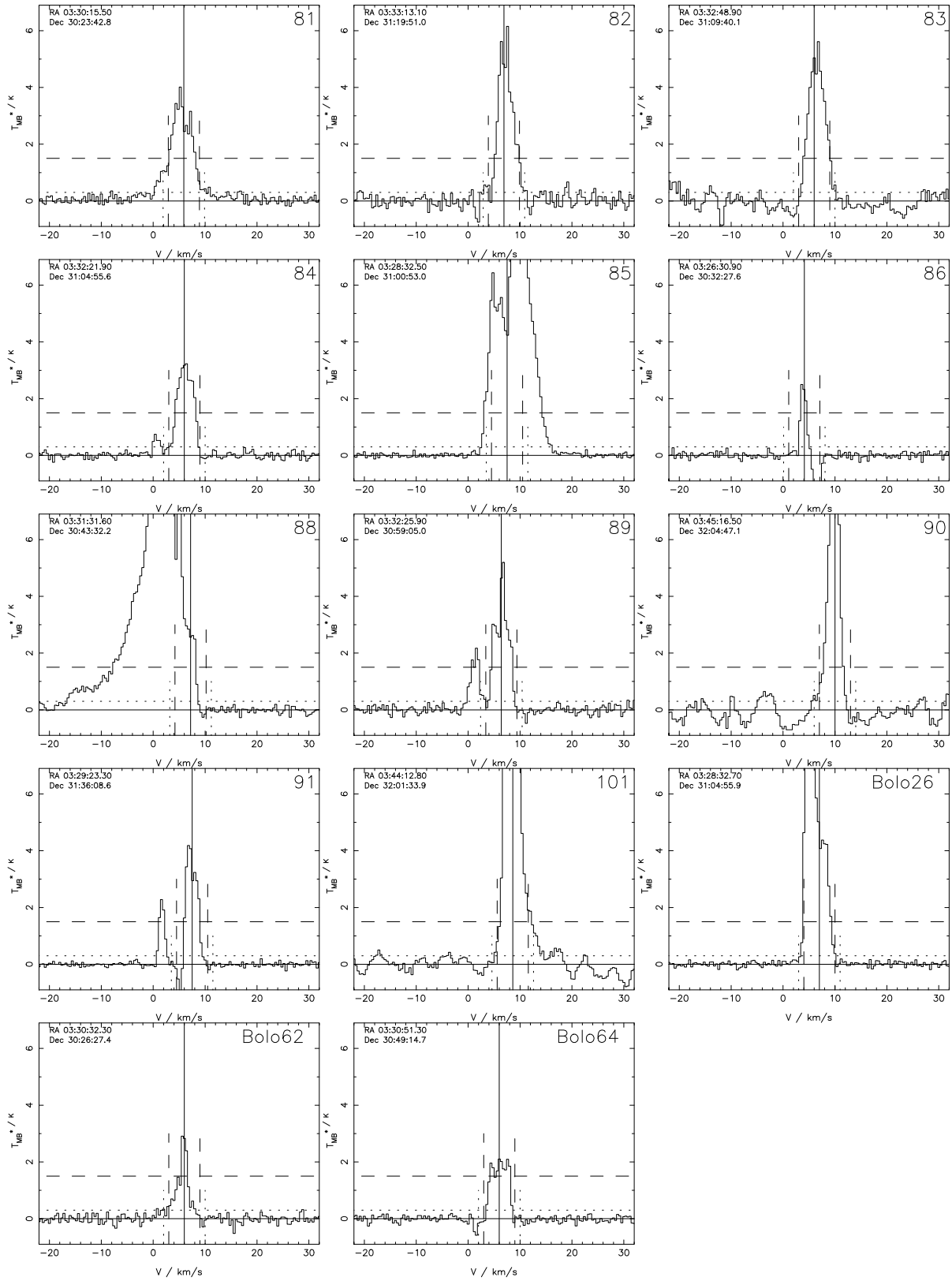
Fig. 8. continued.
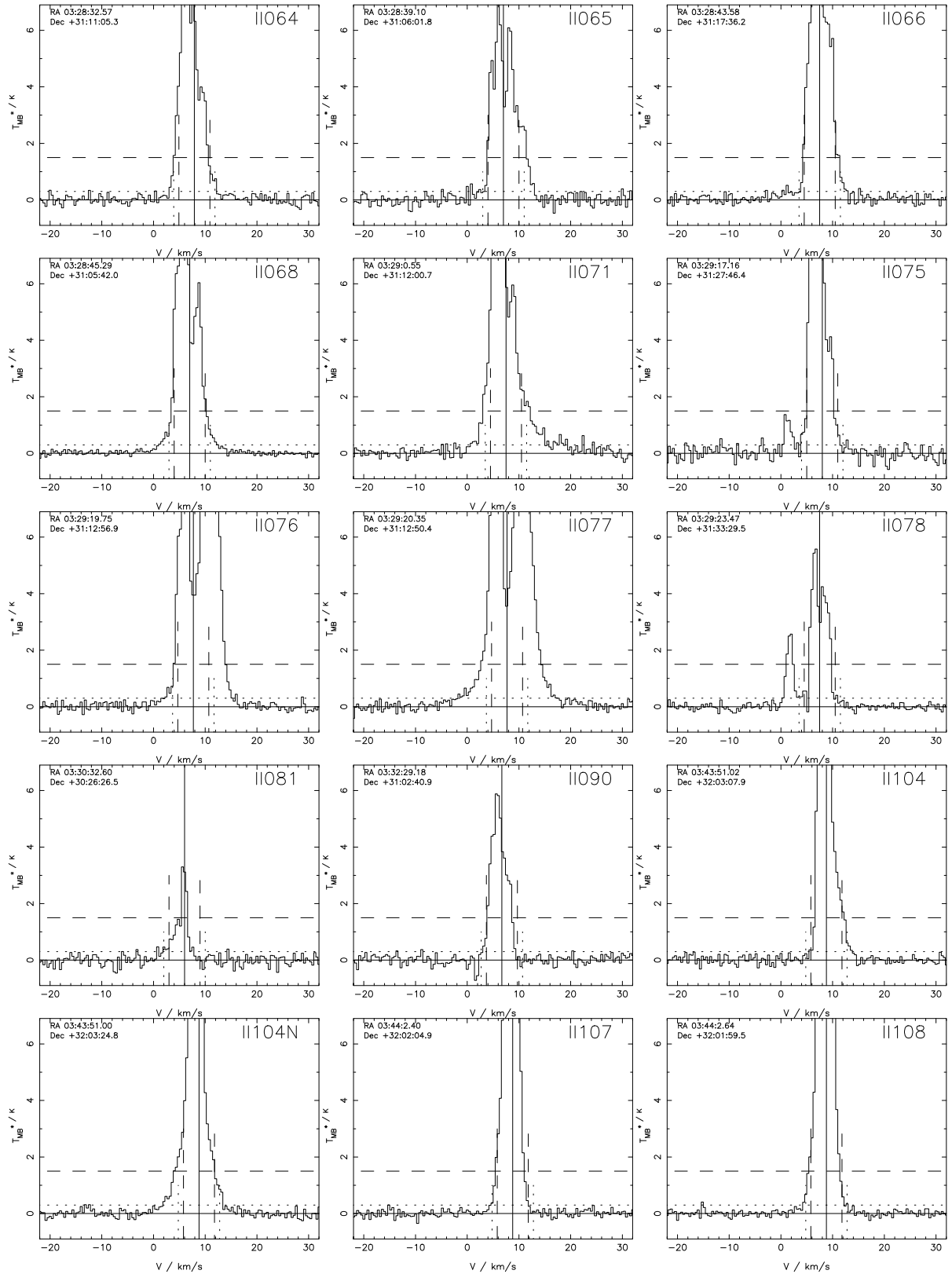
Fig. 9. ^{12}CO spectra at the positions of Spitzer low luminosity objects. See Fig. 8 for annotations. Available in the online version only.

Appendix A: Comments on individual sources and regions

A.1. Low-luminosity objects

LL060 lies in SCUBA core HRF80, southeast of L1448, and is associated with IRAS 03235+3004 (Fig. 6). The core is detected by SHARC, and HARP clearly images the ESE–WNW red–blue outflow associated with this Class I protostar. The outflow is parsec-scale, driving HH317 30″ to the southeast (Davis et al. 2008).

LL064 is associated with SCUBA source HRF75 in the southwest part of NGC1333 (Fig. 5). The core is 2′ south of HRF49, and a compact SHARC-II 350 μm emission peak. The spectrum shows moderate blue and red wings and there is redshifted emission starting at LL064 and extending for the full 3′ northward extent of the map. A potential blue counterpart extends to the SW but requires more extensive mapping to confirm.

The outflow from LL064 is not the most obvious feature in this map. There is also a strong blueshifted lobe lying between the two SCUBA cores, not associated with a dust continuum peak. The blueshifted gas is coincident with a Herbig-Haro object HH744B (Walawender et al. 2005a) and an IRAC source (presumably H_2), and must be the end of an outflow driven by sources to the west, in the south of NGC1333. A good candidate is LL071 (see below).

LL065 and LL068 lie far to the SW of NGC1333 (Fig. 5). LL065 is associated with a loop of submm emission with HRF71 at its NE apex and Bolo26 to the SW. The IRAC emission for LL065 consists of an arc plus a compact source, with the latter detected by SHARC-II. Although the arc may be explained as a H_2 shock, the MIPS and SHARC-II emission suggest that the compact object is protostellar. LL068 (IRAS 03256+3055) lies 1′ to the east of HRF75 and HRF71 and only has a faint SCUBA core (140 mJy/beam, 4σ detection) but is detected as a northeast-southwest ridge by SHARC. Linewings are detected for LL068 and the map shows a clear redshifted lobe running to the east, with widespread blueshifted gas to the west which may be associated with the redshifted Herbig-Haro objects HH340B (Hodapp et al. 2005). LL065 also shows a clear red wing from with emission strongest close to the source but extending to the NW of the map. This outflow could be entirely locally driven by LL065, but possibly it is confused with the flow from LL068 (IRAS 03256+3055). Alternatively, the shocks could be driven by sources in NGC1333 to the north (Davis et al. 2008); this seems a likely explanation for the widespread blueshifted gas in the region, which continues southwest to Bolo26.

LL066 is on the edge of HRF55 (Fig. 5). It is not clearly associated with a SCUBA peak, Dunham et al. (2008) do not classify it as an embedded source, and it shows no SHARC-II emission at a level of 1.6 Jy/beam (3σ). Therefore it is highly unlikely to be a protostar. Nonetheless, it satisfies the linewing criteria and shows red and blueshifted components on the map. There are strong H_2 shocks in this area (Davis et al. 2008). It is very likely that this flow is driven by a source in the main NGC1333 cluster to the northeast. A good candidate is NGC1333 ASR 114 (HRF45), but further mapping is needed to confirm this.

LL071 lies in the southern part of NGC1333 (Fig. 5), to the south of SVS13 and east of IRAS 4, associated with SCUBA HRF65. The submm core lies on a partial dust shell centred to the north which Sandell & Knee (2001) suggest is created by earlier outflow activity. There is compact 350 μm emission at the Spitzer position. The spectrum shows convincing red and blue wings and the outflow is confirmed by the map. To the east, the redshifted flow is initially well collimated but becomes confused with the blueshifted flow from IRAS 4A after 1′. The blueshifted flow to the west is almost immediately confused with the heavyweight blueshifted flows coming south from SVS13 (HRF43) and IRAS 2A (HRF44), detected in H_2 by Davis et al. (2008), and appears to bend to the south. Possible extensions to this flow are seen in the redshifted gas to the south of SCUBA source HRF59 and in the strong blueshifted lobe which lies between HRF49 and HRF74 (see description of LL065).

LL075 and LL078 (HRF61 and HRF58 respectively) lie in the far north of NGC1333 (Fig. 4). Both Spitzer sources are coincident with the SCUBA cores and show strong SHARC-II emission. In LL078 the 350 μm continuum extends 20″ to the southeast. No outflow is detected from LL075, and the flow from LL078 is weak and only detected with the low-level linewing criteria discussed in Sect. 3.1.2. These spectra have a sharply delineated main velocity component between 5 and 11 km s^{-1} corresponding to the $C^{18}O$ line; the second, weak component at 0–3 km s^{-1} is widespread in the north of NGC1333 and probably foreground emission. The cores containing these sources have masses of $\sim$4 $M_\odot$ and were classifed Class 0 (Hatchell et al. 2007b). Like other submm cores in this region, they have filamentary tails pointing away from the main NGC1333 cluster which suggest that they are actively being eroded by the stellar winds from the NGC1333 OB population. To explain the outflow non-detection, the disruption must either have halted accretion (by increasing turbulence or removing the reservoir of gas) or have removed enough gas for the outflow detection to fall below our detection limit. There is no evidence for linewings above 300 mK in HRF61.

LL076/077 both show redshifted and blueshifted emission, strong at the position of LL077. These low luminosity Spitzer sources lie to the north of a submm filament running southeast from IRAS 4 and including HRF72 and HRF59 (Fig. 5). Both are classified in Group 6 by (Dunham et al. 2008) as unlikely to be embedded protostars and indeed there is very little submm emission detected by SCUBA at this position, and none detected by SHARC-II (Fig. 11). The positions of LL076 and LL077 coincide with Herbig-Haro objects HH5A and B respectively, both redshifted (Herbig 1974; Cohen et al. 1991) and extending further to the southeast (Walawender et al. 2005a), and also H_2 2.12 μm emission Davis et al. (2008). This fits with the strong redshifted emission towards both sources, HH5A (LL076) is suggested by Cohen et al. (1991) possibly to harbour the driving source but the absence of SHARC-II emission rules against this. It is more likely that these shocks are driven by NGC1333 IRAS7 5′ to the northwest, as suggested by (Davis et al. 2008). Despite the distant driving source, and the lack of an obvious dust clump to collide with, the strong CO emission is compact both in red and blue (further strong emission to the southwest appears to be independent). The outflow orientation must be more or less along the line of sight to explain the strong blueshifted emission as well as red towards LL077. At the position LL077, HH5B appears as a classic NE–SW arc. These

sources are Herbig-Haro objects which have mimicked embedded protostars in the Spitzer bands.

LL081 lies in the core Bolo62 in the filament to the southwest of B1. The spectra show a weak blueshifted wing which is classified as an outflow only by the low-level criteria. LL081 lies 4′ to the northeast of HRF81 (IRAS 03271+3013), which clearly drives an outflow in this direction (Fig. 3). The weak blueshifted wing at the position of LL081 could be due to this outflow; certainly, nothing in the morphology in the map convinces that LL081 is driving a separate flow. However, there is a strong SHARC-II detection at this position which suggests that this is a real protostar, and the Bolocam detection cannot be due to CO contamination. A higher S/N map would help to confirm the outflow status of this source.

LL090 lies between HRF84 and HRF89 to the west of B1. The alignment strongly suggests that LL090 may drive the blueshifted flow into HRF84 but the spectrum shows only a weak blueshifted linewing. The SCUBA detection is weak but SHARC-II detects a strong peak with a north-south extension. The flatter SED (Fig. 10) suggests that LL090 is a more evolved source, likely Class I, which may explain the relative lack of CO at the source position.

LL104 is associated with IC348 SMM3 (HRF15, Fig. 2). This submm core hosts two Spitzer sources. The southern source is the low luminosity source LL104, but it is apparently the source to the north (here labelled LL104N) which is driving a small and faint molecular outflow (Tafalla et al. 2006), also seen with HARP (Figs. 2 and 9). There is no 70 μm detection for LL104N listed in the c2d catalog, and detection at 70 μm was required for inclusion in the LLO list (Dunham et al. 2008). Inspection of the MIPS image shows there clearly is a 70 μm source, but it lies too close to the brighter LL104 70 μm source to be extracted separately in the c2d pipeline. MIPS and SHARC-II emission suggests that LL104 may also be a second protostar, but any outflow driven by LL104 itself is not evident from the spectra and must be very weak to be confused with the northern flow, which has an estimated mass of only 10^{-3} $M_\odot$. The K-band emission coincident with LL104 takes the form of a bow around the head of the red flow lobe (Tafalla et al. 2006), and it is identified with H$_2$ features (*2a,b* of Eislöffel et al. 2003, , see Fig. 2) though it is not optically-detected Herbig-Haro objects in Perseus; HH795 is 30″ to the west associated with another H$_2$ knot Walawender et al. (2005a); Eislöffel et al. (2003). It is unclear how much of this Spitzer detection is due to H$_2$ shocks.

LL107/108 are interlopers with no outflow. This low luminosity / VeLLO pair 107/108 lies in the horseshoe of dense dust/gas south of IC348, offset 20″ to the NE of the peak of the SCUBA source HRF16 (Fig. 2). The SHARC-II emission peak is separated from the IRAC double detection by 15″ and extends only faintly across to the Spitzer position. The CO spectra shows a slight blue wing (0.5 K at 3 km s^{-1} from line centre), but this is not obviously an outflow as emission at these velocities is widespread in this region in a N-S ridge bowed to the east. The sources LL107/108 are certainly associated with H$_2$ shocks (Eislöffel et al. 2003, *3a,b,e*, see Fig. 2) which may be driven by IC 348 MMS, or the same source as the Flying Ghost Nebula

(Walawender et al. 2006; Eislöffel et al. 2003). These Spitzer sources appear to be HH objects rather than protostars.

A.2. NGC1333 N

The 8′ × 8′ region in the northern part of NGC1333 deserves some further comment. The nearby, young (1 Myr) cluster NGC1333 is the ongoing subject of studies focussing on its stellar content (Wilking et al. 2004; Aspin 2003), dense cores (Walsh et al. 2007; Hatchell et al. 2005; Sandell & Knee 2001), and the relationship between the two (Gutermuth et al. 2008; Enoch et al. 2008; Hatchell et al. 2007b; Jørgensen et al. 2007). In Paper III, Hatchell determined the outflow status of the SCUBA cores in the main dense cluster using the Knee & Sandell (2000) JCMT R×B map. This central region has also now been mapped with HARP and will be discussed elsewhere (Curtis et al. in prep.). Here we concentrate instead on regions of NGC1333 where the outflows have not previously been observed, to the north and south of the main cluster.

The northern part of the NGC1333 region is dominated by the two late-type B stars which power the reflection nebula which gives the region its name. The B5e star SVS3 (Strom et al. 1976; Lada et al. 1996) and, further to the north, B7V BD +30° 549 (Aspin 2003) light up cavities opening northwards away from the main cluster. In terms of the SCUBA cores, SVS3 lies just north of 54 and BD +30° 549 between 57 and 67. These stars strongly heat the gas in this northern region. At the position of SVS3, T_{MB}(^{12}CO 3–2) reaches 50 K; at a position 30″ to the south of BD +30 deg 549, 70 K (Fig. 8), indicating kinetic temperatures at least this large. Thus strong CO lines in this region indicate high temperature gas, rather than large flow masses. The B stars also drive winds with their own influence on the molecular gas.

The simple red/blue integrated intensity maps in Fig. 4 do not do full justice to the velocity structure in the molecular gas, which is additionally shown as channel maps in Fig. A.1. The SCUBA cores are associated with the main molecular component at around 7.5 km s^{-1}, from their C^{18}O velocities (Paper I).

At low velocities of around 2 km s^{-1}, the low column density cloud first discovered by Loren (1976) extends across the north of the map (see sources HRF61, HRF64, HRF58, HRF91 below). This is visible in CO 3–2 above +31°27′ though in ^{12}CO 1–0 it can be seen to extend as far south as +31°22′ at $v = 0$ km s^{-1} increasing in strength and velocity towards the north (Brunt, priv. comm.).

There is a blueshifted gas between 3 and 7 km s^{-1} in the west of the map forming a N-S structure over 4′ in extent with a sharply defined eastern boundary. Peak line intensities are typically 15 K. This component has neither the typical linewings of an outflow nor an obvious driving source. It is possible that it is a fossil flow which has been cut off from a driving source, which could be much further south. An alternative explanation is that winds from BD + 50 459 and SVS3 have excavated a cavity in the molecular gas, and are now heating the inner edge. The morphology of the reflection nebula (Gutermuth et al. 2008) and the dust filaments both suggest that there are strong winds blowing northwards in this region. The highest-velocity redshifted components lie in the centre south of the map, 1′ to the northeast of SVS3.

We discuss the outflow status of individual sources below, but because this region is so complex many of our results are necessarily inconclusive. Embedded YSO identification based on Spitzer colours is difficult because of the high probability of finding reddened background sources, and because much of the
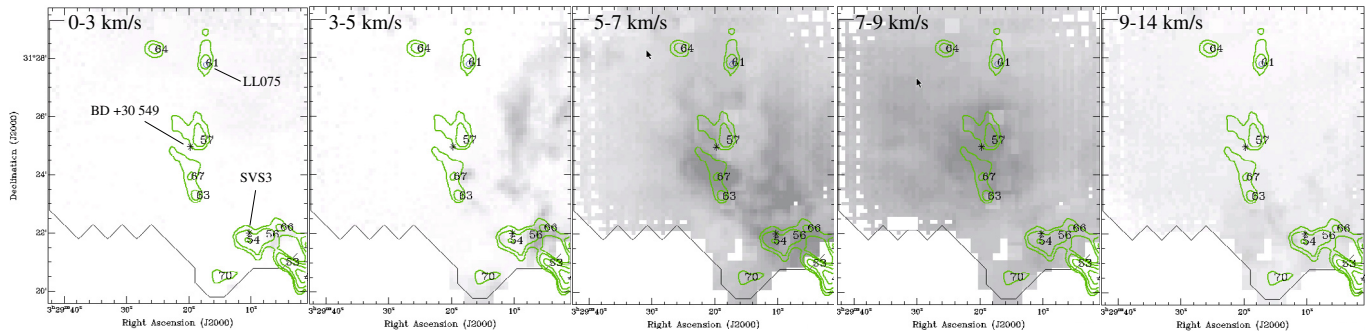
Fig. A.1. Mean intensity maps of NGC1333 N in five velocity ranges as marked. SCUBA cores are numbered and contoured in green at $(1,2,4,8,16,32) \times 100$ mJy/beam (Hatchell et al. 2005, 2007b). The two early-type stars are marked with stars and labelled in the first panel, and the Dunham et al. (2008) low-luminosity source indicated with a circle.

infrared is also saturated by the bright nebula, and there are several differences between Jørgensen et al. (2007) and Gutermuth et al. (2008). The recent Davis et al. (2008) UKIRT H_2 survey only identifies a couple of H_2 knots attributed to the HH6 driving source IRAS7 SM1 4′ to the south.

HRF54, HRF56 and HRF66 This row of submillimetre peaks lies on the northern boundary of the main NGC1333 cluster and just off the (Knee & Sandell 2000) outflow map. Flows northwards from the Class 0 source SK31 (HRF47) and NGC1333 ASR114 (HRF45) to the south may extend across these sources. Looking at the map (Fig. 4) and CO spectra, there is widespread red/blue emission. The blueshifted wing of HRF66 meets the criteria, HRF54 only shows weak wings, but the spectrum for HRF56 clearly shows red and blue wings, also apparent in the maps (Fig. A.1), so this source has all the characteristics of an outflow driving source.

In Hatchell et al. (2007b) we classified HRF54 and HRF56 as Class I and HRF66 as starless. None of the three were identified as protostars by (Jørgensen et al. 2007), but with a different classification of the Spitzer data, Gutermuth et al. (2008) identify a Class I source with HRF56 and another in the filament to the southeast, as well as three without associated SCUBA emission further to the north (see their Fig. 10). The identification of HRF56 as an embedded YSO agrees with its outflow status.

HRF63, HRF67 and HRF57 These cores lie on the northeastern boundary of the reflection nebula. Heated by BD +30° 549 0.1 pc away in projection, 57 and HRF67 may be hotspots rather than true dust cores. Core HRF57 shows no evidence for outflow or embedded infrared sources. The protostellar core HRF63 (Hatchell et al. 2007b; Jørgensen et al. 2007), has evidence for a redshifted flow which extends to the south (Fig. A.1). To its north SCUBA core HRF67, also classified protostellar by Jørgensen et al. (2007) and Paper II but not by Gutermuth et al. (2008), does not classify as an outflow source based on its spectrum. The integrated intensity velocity ranges of -5.5–4.5km s^{-1} (blueshifted) and 10.5–20.5 km s^{-1} (redshifted) also pick up widespread gas components at small blueshifted velocities; CO components out to 10 km are also widespread.

HRF58,HRF61,HRF64 and HRF91 Low-luminosity Spitzer sources LL075 and LL078 were discussed in Sect. A.1. The other SCUBA cores in the filaments extending north from NGC1333, sources HRF64 and HRF91, show no evidence for either embedded protostars or outflow activity.

A.3. NGC1333 S and W

The south and west of NGC1333 contain several sources which lie outside the area covered by Knee & Sandell (2000) and have been targeted by HARP, as shown in Fig. 5. This region contains many low-luminosity sources – LL064,LL065,LL066, LL068, LL071, LL076/77, and LL078 – which are discussed in Sect. A.1 along with the nearby SCUBA cores.

HRF55 and HRF60 show no evidence for outflow from the cores though there is redshifted and blueshifted gas associated with LL066/Gutermuth et al. (2008) Class I source 18, which lies 40″ to the southeast of the SCUBA peak. (Sect. A.1). Gutermuth et al. (2008) Class I sources 16, 19 and 20 also lie 20″ to the south, 3′ to the southeast and 2′ to the east, respectively, so there are plenty of potential driving sources for these outflows.

HRF49 shows a blueshifted wing and blueshifted gas in a NW-SE ridge. Any red counterpart is weak and confused in the map.

HRF65 is discussed with LL071 in Sect. A.1.

HRF59 and 72 are peaks in the dust filament which runs to the southeast from NGC1333 IRAS 4. The most obvious outflow features here are red and blue peaks lying between 59 and 72 and separated by 30″. Neither HRF59 or HRF72 contain driving sources (HRF72 shows no evidence for wings), nor is there another obvious source, from the location of the peaks. The redshifted emission extends to the west and may be driven by LL071 which is 4′ away (HRF65). This explains the redshifted wing at the position of HRF59 (Fig. 5. The blueshifted emission, which has an associated Herbig-Haro object HH759 (Walawender et al. 2005a), is more localised and the driving source is entirely unclear. The infrared images provide few clues, except that the HH object is extended further to the southeast.

HRF69, 71, 75 and Bolo26 are all associated with a loop of continuum emission to the south of NGC1333 which also hosts LL065 and LL068. HRF71 is discussed with LL065 (Sect. A.1). HRF69 and 75 show no linewings by either criterion. There is widespread low-level blueshifted gas in the region which peaks at the position of Bolo26 and at a position between HRF69 and HRF71. The driving source is unclear but is likely to be a source further north in NGC1333. There are several H_2 shocks in this area (Davis et al. 2008, Fig. 8).

HRF85 has linewings which are detected by the low-level crierion. Both the submm continuum and the redshifted CO are arc-shaped opening to the north. The morphology of the blueshifted CO is unclear. An outflow could possibly be driven by nearby Gutermuth et al. (2008) source 13. There are no obvious H$_2$ shocks in this field (Davis et al. 2008).

A.4. IC348 region

Maps of the IC348 region are shown in Fig. 2. The well-known outflows in this region are driven by HH211 (HRF12) and IC348 SMM2 (HRF13).

HRF15 The recently-discovered outflow from IC348 SMM3 (HRF15) (Tafalla et al. 2006) is discussed in detail above (Sect. A.1 source LL104).

HRF101 With HARP, we additionally detect an outflow from the Class I source IC348 LRL 51 (HRF101) with has a compact red lobe.

HRF14,19, 25 and 90 In the extended filaments to the east, HRF14 has a Spitzer YSO (Jørgensen et al. 2007; Gutermuth et al. 2008) and shows an outflow just visible in the HARP maps but discovered with R×B (Paper III), but none of the other SCUBA cores mapped here show outflows or contain Spitzer YSOs.

HRF 16,18,20,21 are the remaining cores in the HH211 horseshoe. They do not house any Spitzer sources except LL107/108 (not protostars, as discussed in Sects. 3.2 and A.1) and do not drive any outflows.

HRF24 and 26 form part of the western filament beyond IC348 SMM3 and are apparently starless.

A.5. B1 region

Per B1 and the filament to the southwest containing IRAS 03271+3013, IRAS 03282+3035 and IRAS 03292+3039 is are shown in Fig. 2. Outflows from the main B1 cluster have been discussed in detail by us (Paper III) and Walawender et al. (2005a). We originally mapped the inner parts of the IRAS 03292+3039 (HRF76), IRAS 03282+3035 (HRF88) and IRAS 03271+3013 flows with R×B but return to the latter two sources with HARP.

IRAS 03282+3035 (HRF88) is discussed in Sect. 3.4 because of its dust continuum emission.

HRF81 (IRAS 03271+3013) has a northeast-southwest outflow (perpendicular to the direction given by (Bachiller et al. 1991)) with a clear outflow cavity in the blueshifted flow to the northeast, and a weaker red counterpart to the southwest. The linewings from this Class I source are weak and only qualify by the low-level criteria. The connection with Bolo52/LL081 to the northeast is discussed in Sect. A.1.

HRF 5,83,84 None of the scattered SCUBA cores show evidence for outflows either in the maps or their linewings. HRF84 shows a fragment of a blueshifted flow which may be driven by LL090 (see Sect. A.1).

HRF82 is identified as a YSO by Jørgensen et al. (2007) though not by Paper II. A possible outflow can be identified by the low-level criterion and as a redshifted flow extending to the north of the SCUBA core. A better signal-to-noise CO map is required to confirm this.

A.6. L1448 and the southwest region

Outflows from L1448 are shown in Fig. 6. The only new HARP map here is HRF32, as outflows from the main sources were mapped with R×B (Paper III) (see also Bachiller et al. 1990, 1991; Wolf-Chase et al. 2000). We also have no new maps to add to the L1455 group, but we have mapped two isolated cores: HRF80 (IRAS 03235+3004) 10′ to the west of L1455, and HRF86 which lies 15′ southeast of L1448.

HRF32 is classified as having an outflow by the low-level crierion but the linewings are almost certainly due to the parsec-scale flow from L1448 N/NW (HRF 27/28) (Wolf-Chase et al. 2000), and there is no Spitzer detection.

HRF86 shows no evidence for protostellar activity.

HRF80 contains an outflow driven by LL060 and is discussed in Sect. A.1.